Hindawi
Shock and Vibration
Volume 2020, Article ID 5498298, 26 pages
https://doi.org/10.1155/2020/5498298

Research Article

Development of Rocking Isolation for Response Mitigation of Elevated Water Tanks under Seismic and Wind Hazards

Hassan Alemzadeh,[1] Hamzeh Shakib ,[1] and Mohammad Khanmohammadi[2]

[1]*School of Civil and Environmental Engineering, Tarbiat Modares University, Tehran, P.O. Box 14115-111, Iran*
[2]*School of Civil Engineering, College of Engineering, University of Tehran, Tehran, P.O. Box 14155-6619, Iran*

Correspondence should be addressed to Hamzeh Shakib; shakib@modares.ac.ir

Received 11 December 2019; Revised 15 August 2020; Accepted 3 September 2020; Published 5 October 2020

Academic Editor: Vasant Matsagar

Elevated water tanks are categorized as strategic components of water supply systems in modern urban management. Past earthquake events have revealed the high vulnerability of these structures. This paper investigates the development of rocking isolation (RI) to these structures as a response mitigation technique. Using an analytical approach, a dynamic model is developed for two isolation cases: (1) at the pedestal base and (2) under the tank. The model incorporates a simplified analogy for simulating the liquid-tank system which is modified for a tank under rocking motions. Based on the dynamics of rocking structures, the equations of motion, impact, and uplift transitions are derived. Then, free vibration and seismic response history analyses are carried out on a sample structure. Discussions are made on the effect of RI on the dynamic and seismic responses of the pedestal and components of the liquid-tank system. Effects of various RI cases, pedestal heights, and tank filling levels are studied for a group of structures excited by an ensemble of ground motions. Considering that the system may be vulnerable to other lateral loadings, the combined effects of seismic and wind hazards are also studied. The wind loads are assumed to act statically and simultaneously with the seismic excitations. Results show that the first case of RI decreases the acceleration demands of mid-rise and tall structures, thus lowering the structural demands to 50% of the fixed-base system. However, the second case of RI has almost no effect on the performance of the system, upgrading only the response of mid-rise structures. Both RI cases also aggravate the wave oscillations and increase the freeboard requirements. Finally, while the combined seismic and wind hazards have almost no effect on the operational performances, the force demands of the structures are increased by 10%.

1. Introduction

Rocking mechanism is a low-damage technology that not only reduces the spread of nonlinear damage to structural components but also mitigates the downtime and repair cost of structures after an earthquake event [1]. Moreover, when the excitation is over, the rocking structure will return to its original position and unlike fixed-base structures, no residual deformations are observed. This also provides resilient behavior against cascading hazards such as multiple aftershocks. These aspects of rocking mechanism, in addition to the ancient structures with unintentional rocking behavior or modern ones equipped with rocking isolation (RI), which performed well during past earthquakes [2, 3], have drawn the attention of many researchers. The first analytical model for a rigid-like structure rocking on a rigid base was proposed by Housner [2] in an effort to investigate the behavior of tall slender structures such as elevated water tanks that survived during the 1960 Chilean earthquakes. It was shown that despite the appearance of instability for these structures, there is a scale effect making the larger structures more stable than smaller ones with similar geometry.

Hereafter, application of this technique to various structural systems like buildings and bridge piers has been the objective of many theoretical [3–11] and experimental studies [5, 8, 12, 13]. Many of these studies showed the remarkable dynamic stability and low-damage capability for both rigid [4–8] and deformable structures [9–13]. This also includes the

studies on assemblies of rocking bodies such as stacked blocks [14], rocking ancient frames and elements [15], and rocking assemblies coupled with SDOF systems such as rocking podium structures [16] or with TMDs [7, 17]. Moreover, there are some studies conducted on the intentional application or development of rocking mechanism for nonbuilding structures such as industrial equipment [18], bridge piers [19], and architectural or art objects [20].

Nevertheless, there are relatively fewer studies on the rocking behavior of liquid storage tanks and even scarce ones on the RI application to tanks. First, there is a handful of studies which investigated the effect of rotational/rocking component of the base excitation on the response of tanks and the fluid-structure interaction (FSI) system [21, 22]. This group of studies has a similar approach to the one that was firstly proposed by Housner [21], i.e., an equivalent analytical model is presented for seismic response analysis of tanks under the action of rocking base excitation. The advantage of this model is the rotational mass component added to the former equivalent mechanical model of the liquid-tank system, which can be used in similar models of rocking tanks. The other category of these studies mainly focuses on the "unintentional" uplift of the bottom plate of ground-supported tanks [23–25] under seismic or dynamic actions. Finally, most of the studies carried on the seismic performance upgrade of storage tanks are involved with the application of slide isolation technique by using elastomeric bearings [26–28] or application of baffled damping plates [29]. Hence, to the knowledge of the authors, there is no study devoted to the "intentional" application of RI mechanism to liquid storage tanks (elevated or else) as a seismic response upgrade strategy. It is noteworthy that the main difference between the unintentional rocking of the structures and the intentional application of RI is that the structure is required to return to its original undeformed position and no sliding or stepping out is allowed, i.e., a necessity for a system with resilient behavior.

Although a detailed investigation of the experimental studies carried on rocking structures is beyond the scope of this paper, some of the recent campaigns [8, 12, 13] showed the difficulties and limitations of these studies. Thus, development of analytical or numerical models for analysis of rocking structures was considered by many researchers. In this regard, multiple FEM-based models are proposed for "rigid" and "deformable" [30–32] rocking structures most of which validate their corresponding analytical models. Accordingly, the authors applied an FEM-based approach [33] using OpenSees framework for seismic analysis of ground-supported tanks with RI which was limited to ground steel tanks. However, this model was not validated by the previous analytical or experimental approaches [23] due to the limitations of the impact modeling techniques. Thus, development of an analytical model for liquid storage tanks with rocking motion is proved to be essential.

To the best of our knowledge, the study by Taniguchi [24] is the only research to partly investigate the rocking behavior of ground-supported tanks using an analytical model. Taniguchi applied a Housner-like [2] approach to the rigid flat-bottom tanks under the action of the horizontal base excitation and derived the equations of the rocking motion. Although he simplified the equivalent analytical model by omitting the sloshing or convective component from the liquid-tank system and assuming the tank wall flexibility component only, the total liquid mass is assumed for studying the global stability of the structure. Moreover, the effect of impacts at the rocking interfaces on the response of the structure is not discussed in his model.

Initially, this paper focuses on addressing the shortcomings of Taniguchi's model and further developing this model for planar (2D) seismic analysis of intentionally rock-isolated elevated tanks under horizontal and vertical base excitations. For this purpose, firstly the equations and systematic approach used in the aforementioned studies are reviewed. Then, the general assumptions made for the developed model of rocking elevated tanks are presented. Moreover, the effects of impacts at rocking interfaces on the global responses are revisited. A numerical algorithm is also presented for solving the equations of motions which appears to be less time-consuming in some specific prototypes with mathematically "stiff" equations.

Hereafter, another objective of the paper is to obtain basic information on the applicability and effectiveness of RI as a seismic response upgrade technique. Thus, following a similar approach applied in previous studies on slide-isolated elevated tanks or similar structures [26–28, 34], two cases of RI are investigated: (1) isolation at the base and (2) isolation under the tank. In both cases, the elevated tanks are assumed to be located on stiff soil sites and soil-foundation interaction is neglected. Considering that the proposed system may be vulnerable to other lateral loadings, the combined effects of seismic and wind loads are also studied. The wind loads are assumed to act statically and simultaneously with the seismic excitations. Accordingly, parametric studies are carried out on a group of prototypes with various pedestal/shaft heights and tank filling levels which are analyzed under the combined action of seismic and wind hazards.

2. Analytical Model of the Rocking Elevated Tank

2.1. Review of Similar Analytical Models. Firstly, by applying the same assumptions applied in Housner's analytical model [2], the equation of rocking motion for a 2D homogenous rigid block with an aspect ratio of α and a diagonal of length $2R$ under the horizontal and vertical base excitation is as follows:

$$I_o\ddot{\theta} = -m\left(g + \ddot{u}_g^Y\right)R\sin\left[\alpha\mathrm{sgn}\theta(t) - \theta(t)\right] - m\ddot{u}_g^X(t)R\cos\left[\alpha\mathrm{sgn}\theta(t) - \theta(t)\right], \quad (1)$$

where θ is the rotational response of the block, m is the total mass of the block, and I_O is the rotational mass inertia of the block about one of its pivot points (O or O′). Also, $\ddot{u}_g^X$ and $\ddot{u}_g^Y$ are, respectively, the horizontal and vertical components of base acceleration.

Taniguchi [23] applied the same approach to a ground-supported steel tank under horizontal base excitation (Figure 1). Considering only the first vibration mode of the liquid-tank system, the equations of planar rocking motion are derived as follows:

$$I_o\ddot{\theta} = -M_O g R_O \sin\left[\alpha_O - \theta(t)\right] + \mathrm{sgn}\theta(t) H_I \left(C_I \dot{x}_I + K_I x_I\right), \tag{2}$$

$$M_I \ddot{x}_I - \mathrm{sgn}\theta(t) M_I g \sin\theta + \mathrm{sgn}\theta(t) M_I R_I \dot{\theta}^2 \sin\alpha_I + \mathrm{sgn}\theta(t) M_I R_I \ddot{\theta} \cos\alpha_I + M_I \ddot{u}_g^X \cos\theta + C_I \dot{x}_I + K_I x_I = 0, \tag{3}$$

where M_I, K_I, and C_I are, respectively, the mass, stiffness, and damping coefficients corresponding to the first vibration mode of the liquid-tank system and x_I is the first mode displacement response. Also, θ is the rocking response of the tank. Finally, M_O and I_O are, respectively, the mass and rotational mass inertia of all tank liquid about one of its pivot points (O or O′).

Regarding its assumptions and approach, Taniguchi's model has the following shortcomings:

(i) Including the total values of liquid mass M_O and its rotational inertia I_O in equation (2) unrealistically stabilizes the tank during rocking motion and thus produces smaller and nonconservative values for rotational and translational responses. Accordingly, researchers have shown that proportions, and not the total values, of these parameters especially for I_O should be used in the analysis of rocking tanks [21, 22] disregarding the rigidity of the bottom plate.

(ii) The effect of the convective component of the liquid-tank system is not included in this model, which, as discussed later, shows notable effects on the global dynamic stability and rocking and displacement responses of rocking elevated tanks.

(iii) The details of the analytical model for including the effect of the impacts at rocking interfaces on the postimpact responses of the tank are not discussed in this model and only an imperfect restitution coefficient (e), the value and calculation method of which is not clarified, is used for determination of postimpact rotational response.

(iv) Change in the pressure responses acting on the tank wall due to the rocking motion of various components of the system is not studied.

Observing the aforementioned remarks, one of the main goals of this paper is to focus on resolving these shortcomings and develop the model for seismic analysis of rocking elevated tanks.

2.2. General Assumptions of the Developed Model. As mentioned before, a rocking elevated tank with shaft staging is studied in this paper. Two cases of RI at different levels are presumed for this structure: (C1) at the base or under the pedestal/shaft (Figure 2) and (C2) under the tank or top of the pedestal (Figure 3). As shown Figures 2 and 3, the liquid-tank system is modeled by an equivalent mechanical analogy including lumped masses, springs, and dashpots. Properties of this simplified model which is a combination of analytical approaches presented by Housner [35], Haroun [36], and Haroun and Ellaithy [21] are shown in Figure 4. The main advantage of this analogy is its ability to study the combined effect of translational and rocking motions on the response of the liquid-tank system. This is mainly accomplished by considering a modified rotational inertia (I_r) for the liquid-tank impulsive/rigid component which is of great importance in analyzing systems experiencing rocking motions. In Figures 2–4, the subscripts of "C", "1," and "0" describe the "full-contact" geometrical properties (aspect ratio, α, and radial distance to the pivot points, R) of the masses corresponding to the convective, wall flexibility, and impulsive components of the simplified liquid-tank system, respectively. Similarly, the subscripts of "r", "f," and "S" correspond to the tank roof, tank floor, and supporting shaft centers of gravity (C.G.). H_L is also the filling level of the "liquid." Moreover, the following assumptions are made while analyzing both RI cases:

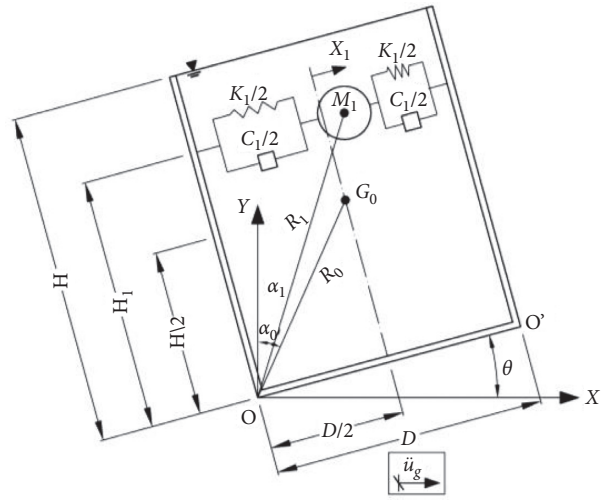

Figure 1: Analytical model for the rocking behavior of ground-supported tanks presented by Taniguchi [23].

(i) The tank structure storing liquid and its components including roof slab, floor slab, and its framing beams and also the foundation of the structure are assumed to be rigid. However, in all cases, the supporting/shaft structure is assumed to be laterally deformable. The tank wall flexibility is also considered via the aforementioned simplified liquid-tank system (Figure 4).

(ii) The liquid-tank system is assumed to be fully constrained with the tank structure in the perpendicular direction of the floor, and its components move rigidly with the tank wall in that direction.

(iii) For the system to be resilient, the rocking body (shaft in C1 or tank in C2) is constrained not to slide or roll out of its initial position. This constraint is

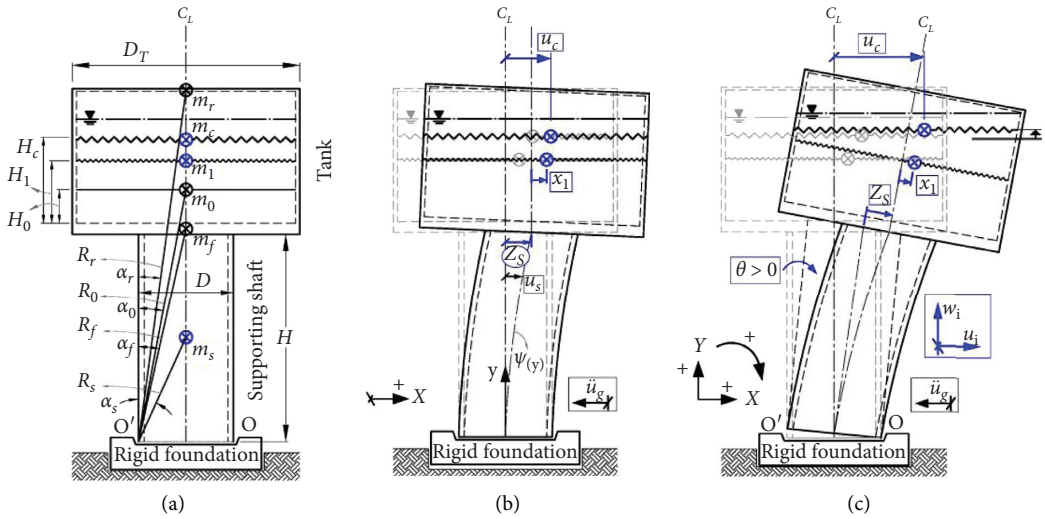

FIGURE 2: Configuration of rocking elevated tank model with isolation at the base (C1): (a) initial position; (b) preuplift phase of motion; (c) under rocking motion.

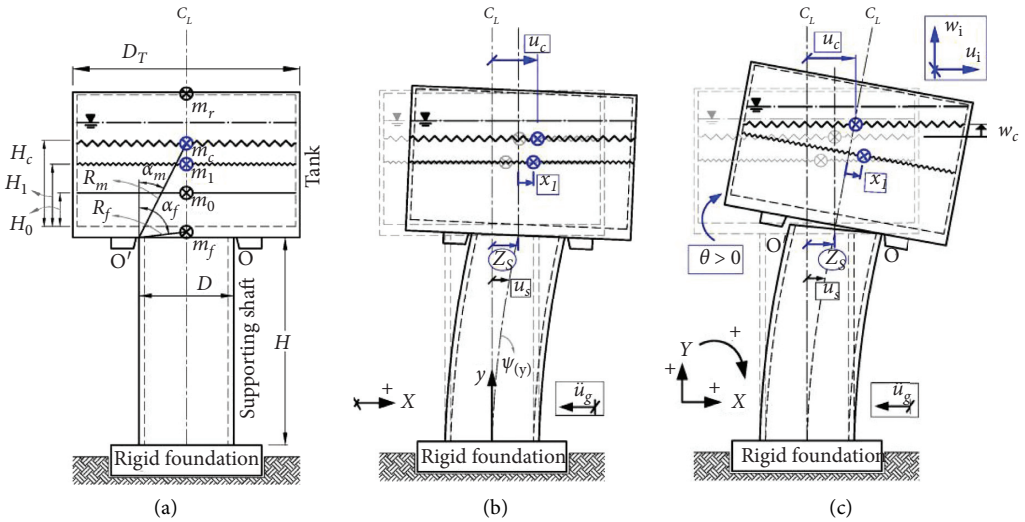

FIGURE 3: Configuration of rocking elevated tank model with isolation under the tank (C2): (a) initial position; (b) preuplift phase of motion; (c) under rocking motion.

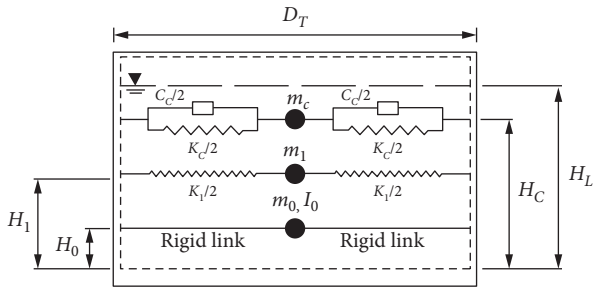

FIGURE 4: Mechanical analogy of the simplified liquid-tank system for a tank under combined translational and rocking motion.

assumed to be a shear key provided at the interfaces. In the first case (C1), the shear key is provided in the foundation and under the bottom of the shaft (Figure 2). For the second case (C2), a similar shear key is assumed in the bottom face of the tank floor and over the top of the shaft. These shear keys are assumed to ensure the direct transformation of shear forces and deformations between the shaft and the foundation or tank.

(iv) The structures are assumed to be located on stiff soil sites (class B or C according to ASCE 7-16 [37]), and soil-foundation interaction is negligible. Specifically, it is assumed that in the first case of RI, the structure rocks on a rigid foundation which is fully constrained to the bottom soil.

(v) The rocking or contact surfaces in both isolation cases are assumed to remain intact and without crushing during the rocking motion. Moreover, sliding is constrained on these surfaces.

(vi) The impact effects on postimpact response condition of the structure and energy dissipations are mainly based on assumptions of Housner's analytical approach [2] and other following researchers such as Chopra and Yim [4] and Vassiliou et al. [10]. More detailed assumptions are presented and discussed for each RI case.

2.3. Preuplift Phase of Motion and Uplift Transition. The first class of equations needed for analyzing the rocking structure includes (1) equations of motion in the preuplift/full-contact phase and (2) uplift initiation equation which is usually defined as a conditional equation for the minimum horizontal acceleration needed to initiate rocking of the structure. As shown in Figures 2(b) and 3(b), in the preuplift phase, the system acts like a fixed-base structure and has three degrees of freedom that are u_C (total displacement of the convective mass), x_1 (relative displacement of the wall flexibility mass), and z_S (flexural deformation of shaft top end). Therefore, the motion of the system is described by the following system of differential equations:

$$\begin{bmatrix} m_C & 0 & 0 \\ 0 & m_1 & m_1 \\ 0 & 0 & \widetilde{m}_S + m_{\text{imp}} \end{bmatrix} \begin{bmatrix} \ddot{u}_C \\ \ddot{x}_1 \\ \ddot{z}_S \end{bmatrix} + \begin{bmatrix} C_C & 0 & -C_C \\ 0 & C_1 & 0 \\ -C_C & -C_1 & \widetilde{C}_S + C_C \end{bmatrix} \begin{bmatrix} \dot{u}_C \\ \dot{x}_1 \\ \dot{z}_S \end{bmatrix} + \begin{bmatrix} K_C & 0 & -K_C \\ 0 & K_1 & 0 \\ -K_C & -K_1 & \widetilde{K}_S + K_C \end{bmatrix} \begin{bmatrix} u_C \\ x_1 \\ z_S \end{bmatrix} = -\ddot{u}_g^X \begin{bmatrix} m_C \\ m_1 \\ \widetilde{L}_S + m_{\text{imp}} \end{bmatrix}, \tag{4}$$

where m_C, C_C, and K_C are the mass, damping, and stiffness coefficients corresponding to the convective component of response in the liquid-tank system, respectively. Similarly, m_1, C_1, and K_1 are the mass, damping, and stiffness coefficients of the wall flexibility component. The mass of impulsive components, i.e., roof m_r, floor m_f, and m_0, is also summarized in m_{imp}. Also, $\widetilde{m}_S$, $\widetilde{C}_S$, $\widetilde{K}_S$, and $\widetilde{L}_S$ are the generalized mass, damping coefficient, stiffness coefficient, and excitation coefficient of the shaft, respectively, which are defined by assuming the shaft as a generalized SDOF system. Thus, lateral deformation of the shaft top end ($z_S(t)$) is assumed as the generalized coordinate of the shaft with uniform mass and flexural stiffness.

Following the previous studies, the uplift criterion for the planar rocking of a rigid block is derived by equating the static overturning and restoring moments about one of the pivot points. However, for the rocking elevated tank, the presence of the liquid-tank system in addition to the system geometrical and mechanical properties modifies this equation. According to Figure 2, the overturning (M_{OT}) and restoring moment (M_{RT}) of the forces acting on the whole structure with C1 during the preuplift phase and immediately before uplift are as follows:

$$M_{\text{OT}} = -\left(\ddot{u}_g^X + \ddot{z}_S\right)\left(\sum_{i=0,r,f} m_i R_i \cos\alpha_i\right) - \int_0^H \left[\ddot{z}_S \psi(y) + \ddot{u}_g^X\right] \text{ydm} - \sum_{j=1,C} m_j R_j \cos\alpha_j \left(\ddot{u}_g^X + \ddot{u}_j\right), \tag{5}$$

$$M_{\text{RT}} = \left(g + \ddot{u}_g^Y\right)\left[\sum_{i=0,r,f} m_i\left(\frac{D}{2} \mp z_S\right) + m_S\left(\frac{D}{2} \mp 0.363 z_S\right) + \sum_{j=1,C} m_j\left(\frac{D}{2} \mp u_j\right)\right], \tag{6}$$

where D, $m_{(i/j)}$, $\alpha_{(i/j)}$, and $R_{(i/j)}$ are the parameters used for the definition of mass and different geometrical properties of various components of the structure ($i = r, f, S$) and the liquid-tank system ($i = 0, j = 1, C$) (Figure 2). Also, considering the relative displacement of the flexibility mass, x_1, one can obtain in the preuplift phase: $u_1 = x_1 + z_S$. By equating these, the rocking criterion is determined as follows:

$$\begin{aligned} |M_{\text{OT}}| > M_{\text{RT}} \Longrightarrow & \left| -\left(\ddot{u}_g^X + \ddot{z}_S\right)\left(\sum_{i=0,r,f} m_i R_i \cos\alpha_i\right) - m_S H\left(0.269\ddot{z}_S + \frac{1}{2}\ddot{u}_g^X\right) - \sum_{j=1,C} m_j R_j \cos\alpha_j \left(\ddot{u}_g^X + \ddot{u}_j\right)\right| \\ & > \left(g + \ddot{u}_g^Y\right)\left[\sum_{i=0,r,f} m_i\left(\frac{D}{2} \mp z_S\right) + m_S\left(\frac{D}{2} \mp 0.363 z_S\right) + \sum_{j=1,C} m_j\left(\frac{D}{2} \mp u_j\right)\right], \end{aligned} \tag{7}$$

where m_S is the total mass of the shaft. The upper signs in equations (5)–(7) correspond to uplift about the right pivot point ($\ddot{u}_g^X < 0$) and vice versa. Accordingly, for C2, external forces acting on the shaft are omitted and the effect of its deformability is considered as follows (Figure 3(b)):

$$\left|-\left(\ddot{u}_g^X + \ddot{z}_S\right)\left(\sum_{i=0,r,f} m_i R_i \cos\alpha_i\right) - m_C R_C \cos\alpha_C\left(\ddot{u}_g^X + \ddot{u}_c\right) - m_1 R_1 \cos\alpha_1\left(\ddot{u}_g^X + \ddot{x}_1 + \ddot{z}_S\right)\right| > \left(g + \ddot{u}_g^Y\right)\left\{\left(\frac{D}{2}\right)\left(\sum_{i=0,r,f} m_i\right) + m_C\left[\left(\frac{D}{2}\right)\mp\left(u_C - z_S\right)\right] + m_1\left[\left(\frac{D}{2}\right)\mp\left(x_1\right)\right]\right\}. \tag{8}$$

2.4. Equations of Rocking Motion. After the initiation of rocking, the motion of the system in both cases of RI is described by four degrees of freedom: θ (rocking response), u_C (horizontal displacement of the convective mass), x_1 (relative displacement of the flexibility mass), and z_S (relative displacement of the shaft top end). The equations of motion (EOM) are derived using Lagrangian formulation:

$$\frac{d}{dt}\left(\frac{\partial T}{\partial \dot{q}_i}\right) - \left(\frac{\partial\left(T - V\right)}{\partial q_i}\right) = Q_{q_i} = \left(\frac{\partial W}{\partial q_i}\right), \tag{9}$$

where T and V are the kinetic and potential energy of the system, respectively, and Q_{q_i} is the nonconservative force acting along the DOF q_i, which for the studied model is the damping forces of various component. The latter is determined by the variation of work (δW) done by the nonconservative force during an admissible virtual displacement of δq_i:

$$Q_{q_i} = \left(\frac{\partial W}{\partial q_i}\right) \equiv \left(\frac{\delta W}{\delta q_i}\right). \tag{10}$$

Equation (9) is also known as Lagrange's EOMs which are a direct result of applying Hamilton's variational principle [38] to all systems (linear or nonlinear) with a specific condition: that the energy and work terms can be expressed by the selected DOFs (q_i), their time derivatives, and also their variations ($\dot{q}_i$ and δq_i).

Placing origin of the axis at the centerline of the shaft on its base (Figure 2(c)), total displacement field of various components of the system with C1 is given by the following expressions:

$$\begin{aligned} u_i &= R_i\left(\sin\left[\operatorname{sgn}\left(\theta\right)\alpha_i\right] - \sin\left[\operatorname{sgn}\left(\theta\right)\alpha_i - \theta\right]\right) + z_S\cos\theta, \quad i = 0, r, f, m, \\ w_i &= R_i\left(\cos\left[\operatorname{sgn}\left(\theta\right)\alpha_i - \theta\right] - \cos\left[\operatorname{sgn}\left(\theta\right)\alpha_i\right]\right) - z_S\sin\theta, \quad i = 0, r, f, m. \end{aligned} \tag{11}$$

It is worth to note that the subscript m stands for the equal-displacement point m representing the tank wall at the level of the convective mass (Figure 5). Similarly, for C2, displacement field of the tank is obtained by following expressions:

$$u_i = z_S + R_i\left(\sin\left[\operatorname{sgn}\left(\theta\right)\alpha_i\right] - \sin\left[\operatorname{sgn}\left(\theta\right)\alpha_i - \theta\right]\right), \quad i = 0, r, f, m, \tag{12}$$

$$w_i = R_i\left(\cos\left[\operatorname{sgn}\left(\theta\right)\alpha_i - \theta\right] - \cos\left[\operatorname{sgn}\left(\theta\right)\alpha_i\right]\right), \quad i = 0, r, f, m. \tag{13}$$

The equal-displacement "point" m is a virtual point assumed to be located at the level of the convective mass with equal distance from the tank walls and moves rigidly with them (Figure 5(b)). The location of this point is of great importance in simplification and describing the terms of convective damping and potential energy of the liquid-tank system. Moreover, considering assumptions of the simplified model introduced in Figure 5 and observations made in some experimental programs [23], the convective mass link to the tank wall is presumed to remain horizontal during rocking motions.

Accordingly, for C1, the total displacement field of the tank wall flexibility component including the relative displacement (x_1) measured in its normal direction (Figure 2(c)) is as follows:

$$\begin{aligned} u_1 &= R_1\left(\sin\left[\operatorname{sgn}\left(\theta\right)\alpha_1\right] - \sin\left[\operatorname{sgn}\left(\theta\right)\alpha_1 - \theta\right]\right) + \left(x_1 + z_S\right)\cos\left(\theta\right), \\ w_1 &= R_1\left(\cos\left[\operatorname{sgn}\left(\theta\right)\alpha_1 - \theta\right] - \cos\left[\operatorname{sgn}\left(\theta\right)\alpha_1\right]\right) - \left(x_1 + z_S\right)\sin\left(\theta\right), \end{aligned} \tag{14}$$

where the term $x_1 + z_S$ is equal to the selected DOF for the flexibility component (z_1). Now, by applying equation (9) to the first DOF (u_C), first EOM for C1 is as follows:

$$\begin{aligned} \ddot{u}_C &- \left(\frac{1}{2}\right)\left\{\dot{\theta}^2\left[2u_C - \operatorname{sgn}\left(\theta\right)D\right] + 2\dot{\theta}\dot{z}_S\sin\theta\right\} \\ &+ \omega_C^2\left[u_C - R_m\left(\sin\left[\operatorname{sgn}\left(\theta\right)\alpha_m\right] - \sin\left[\operatorname{sgn}\left(\theta\right)\alpha_m - \theta\right]\right)\right. \\ &\left. - z_S\cos\theta\right] + 2\xi_C\omega_C\left(\dot{u}_C - R_m\dot{\theta}\left(\cos\left[\operatorname{sgn}\left(\theta\right)\alpha_m - \theta\right]\right)\right. \\ &\left. - \dot{z}_S\cos\theta + z_S\dot{\theta}\sin\theta\right) = -\ddot{u}_g^X, \end{aligned} \tag{15}$$

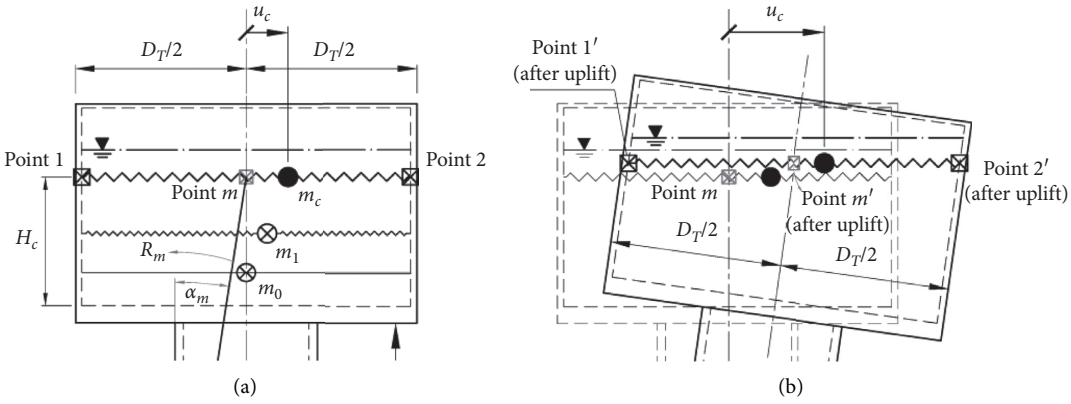

Figure 5: Geometrical properties used in analysis of the tank structure, specifically, the location of virtual point (m) (a) before and (b) after uplift.

where ω_C and ξ_C are the equivalent fundamental frequency and viscous damping ratio corresponding to the convective component of the liquid-tank system, respectively. The other EOM corresponding to the second DOF (x_1) is also obtained as follows for C1:

$$\begin{aligned}&\ddot{x}_1 + \ddot{z}_S + 2\xi_1\omega_1\dot{x}_1 + \omega_1^2 x_1 + R_1\ddot{\theta}\cos\left[\operatorname{sgn}(\theta)\alpha_1\right] \\ &\quad - \dot{\theta}^2\left(z_S + x_1 - R_1\sin\left[\operatorname{sgn}(\theta)\alpha_1\right]\right) + \ddot{u}_g^X\cos\theta \\ &\quad -\left(g + \ddot{u}_g^Y\right)\sin\theta = 0,\end{aligned} \tag{16}$$

where ω_1 is the fundamental frequency of the tank wall flexibility component.

Equations (14) and (15) are similarly developed for C2 considering the displacement field described by equations (12) and (13). For the sake of brevity, these EOMs in addition to the ones corresponding to the third and fourth DOFs, i.e., z_S and θ, are presented in [39]. It should be noted that for C1, by omitting the rotational responses ($\ddot{\theta}$, $\dot{\theta}$, and θ) from equations (15) and (16), the EOMs in preuplift phase (equation (4)) and rocking initiation equation (equation (7)) are reproduced. This gives the second class of equations needed for analyzing the rocking elevated tanks under horizontal and vertical base excitations.

2.5. The Impact Effects. Among important issues to be addressed about rocking structures are the impacts at the rocking surfaces and modification methodology of the postimpact responses of the structure. These specifically include the postimpact velocities of the 4 DOFs of the structure. The continuation of the rocking motion after each impact "event" directly relates to the calculation of these responses as the "next" initial values of the motion. The postimpact motion of the structure is analyzed by the same EOMs, but by using the new initial values obtained from the "immediate" postimpact state. Although various analytical models for the impact transitions of rocking structures have been proposed by many researchers [2, 4, 8–10], the main assumptions of most of these models are almost as follows: (1) the impact transitions are inelastic, (2) the impact transitions and the change of rocking corners are instantaneous, and (3) the impact forces are concentrated at the new pivot point (impacting corner). Following an approach firstly mentioned by Meek [40] and extended by Vassiliou et al. [10], it is observed to be more conservative to presume the impacts to be "perfectly" inelastic with no bouncing. It means that at each impact event, the structure sticks to the rocking interface in a "full-contact" phase and the vertical component of the shaft velocity is damped out. Hence:

$$\theta_2 = \dot{\theta}_2 = 0, \tag{17}$$

where the index "2" corresponds to the postimpact state. Moreover, the conservation of linear momentum (COLM) of the whole system along the horizontal direction gives an equation for the postimpact velocity of the shaft, $\dot{z}_{S,2}$. For C1, it is given by (Figures 6(a) and 6(b))

$$\left(\dot{z}_{S,2} - \dot{z}_{S,1}\right)\left(\widetilde{L}_S + \sum_{i=0,r,f} m_i\right) + \left(-\dot{\theta}_1\right)\left[\left(\frac{m_S H}{2}\right) + \sum_{i=0,r,f} m_i R_i\cos\alpha_i\right] + \sum_{j=1,C} m_j\left(\dot{u}_{j,2} - \dot{u}_{j,1}\right) = 0, \tag{18}$$

where m_S is the total mass of shaft. All other parameters have been defined and shown in Figures 2(a), 6(a), and 6(b). Removing effect of the rocking shaft also gives the following equation for C2:

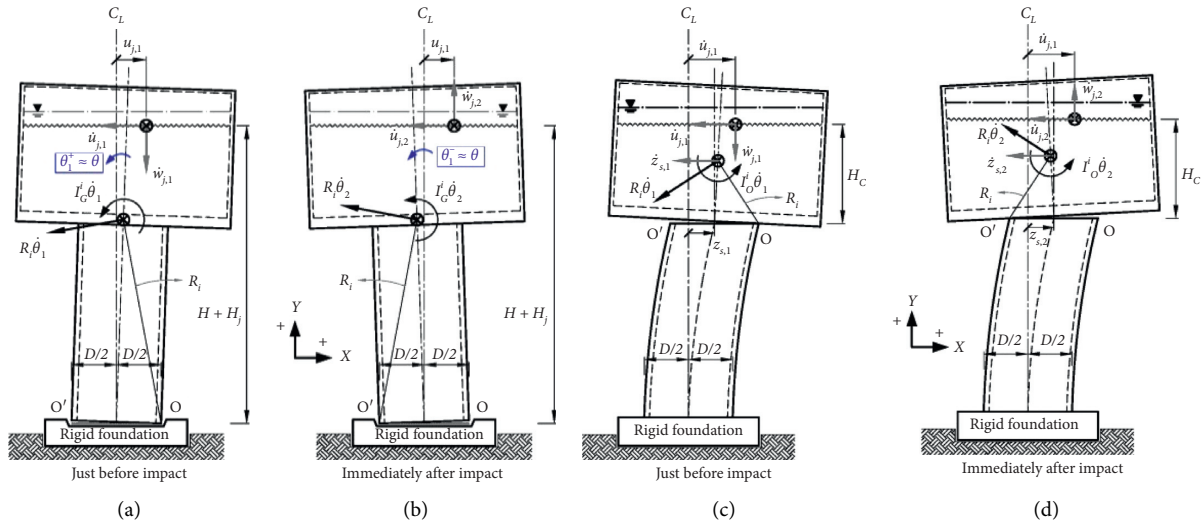

FIGURE 6: Configuration of the rocking elevated tanks with (right) C1 and (left) C2: (a, c) just before and (b, d) immediately after the impact at the left corner (O′).

$$\left(\dot{z}_{S,2}-\dot{z}_{S,1}\right)\left(\tilde{L}_S+\sum_{i=0,r,f} m_i\right)+\left(-\dot{\theta}_1\right)\left(\sum_{i=0,r,f} m_i R_i\cos\alpha_i\right)+\sum_{j=1,C} m_j\left(\dot{u}_{j,2}-\dot{u}_{j,1}\right)=0. \tag{19}$$

It should be noted that the velocity field of the above components is derived from different displacement fields of the corresponding RI cases. Regarding the 4 DOFs of the system, two more equations are needed to find the post-impact responses. The other two impact conditions are based on this assumption that the relative velocities between the convective and flexibility components and the tank structure do not change before and after an impact. Thus:

$$\left(\dot{u}_C-\dot{u}_m\right)_1=\left(\dot{u}_C-\dot{u}_m\right)_2, \tag{20}$$

$$\left(\dot{x}_1\right)_1=\left(\dot{x}_1\right)_2. \tag{21}$$

By solving the equations (17)–(21) simultaneously, one can obtain the postimpact responses of the rocking elevated tank. Accordingly, the transition of the motion to other phases is chosen by substituting these responses in equation (7) or (8), which can be the continuation of rocking motion (Section 2.4) or restart of the preuplift phase of motion (Section 2.3). It is worth to note that by adopting $m_C = m_1 = 0$ in C2, a set of equations similar to those presented in [6] for a rocking block standing free on a seismically isolated base is derived.

2.6. Validation of the Analytical Model. The analytical approach used in this study basically originates from the approach which was first introduced by Housner [2] and later was developed in other studies, such as Meek [40], Chopra and Yim [4], and Spanos et al. [14]. Although rigorous FEM models for rocking structures are much more developed in recent years, these models still needed an acceptable benchmark to be compared and validated with. Due to the difficulties and limitations of experimental campaigns [8, 12, 13, 23, 31], this benchmark was usually chosen from well-established analytical problems to test the numerical model in the limit case [10, 16, 17, 31].

Accordingly, although the present work is not completely new, the approach itself was the first step in a validation process. The authors used this approach and also experimental campaigns [33, 39] to validate and improve a previously introduced FEM model [33].

Nevertheless, some verifications were also conducted [39] based on the result of similar analytical problems. For the first case of RI (C1), by removing the convective and flexibility components ($m_C = m_1 = 0$), the results were verified by those presented for a deformable cantilever structure rocking on a rigid surface [10]. Similarly, the analytical model developed for C2 was compared well with that of a rocking block standing free on a seismically isolated base [6].

3. Procedure of the Numerical Solution

Despite some differences between the RI system and its governing equations studied in this paper, the algorithm of the analysis (Figure 7) is basically similar to that of other rocking structures [4, 8, 10]. Nevertheless, there are some modifications. Firstly, the EOMs are integrated numerically using "ode45" solver package of MATLAB [41]. This package is based on an explicit Runge–Kutta (4, 5) formula, namely, the Dormand–Prince pair [42], which is a one-step differential equation solver needing only the solution at the immediately preceding time point. During each phase of the motion, the EOMs are integrated using the initial state value (IVs) of each component, including initial displacement and velocity fields.

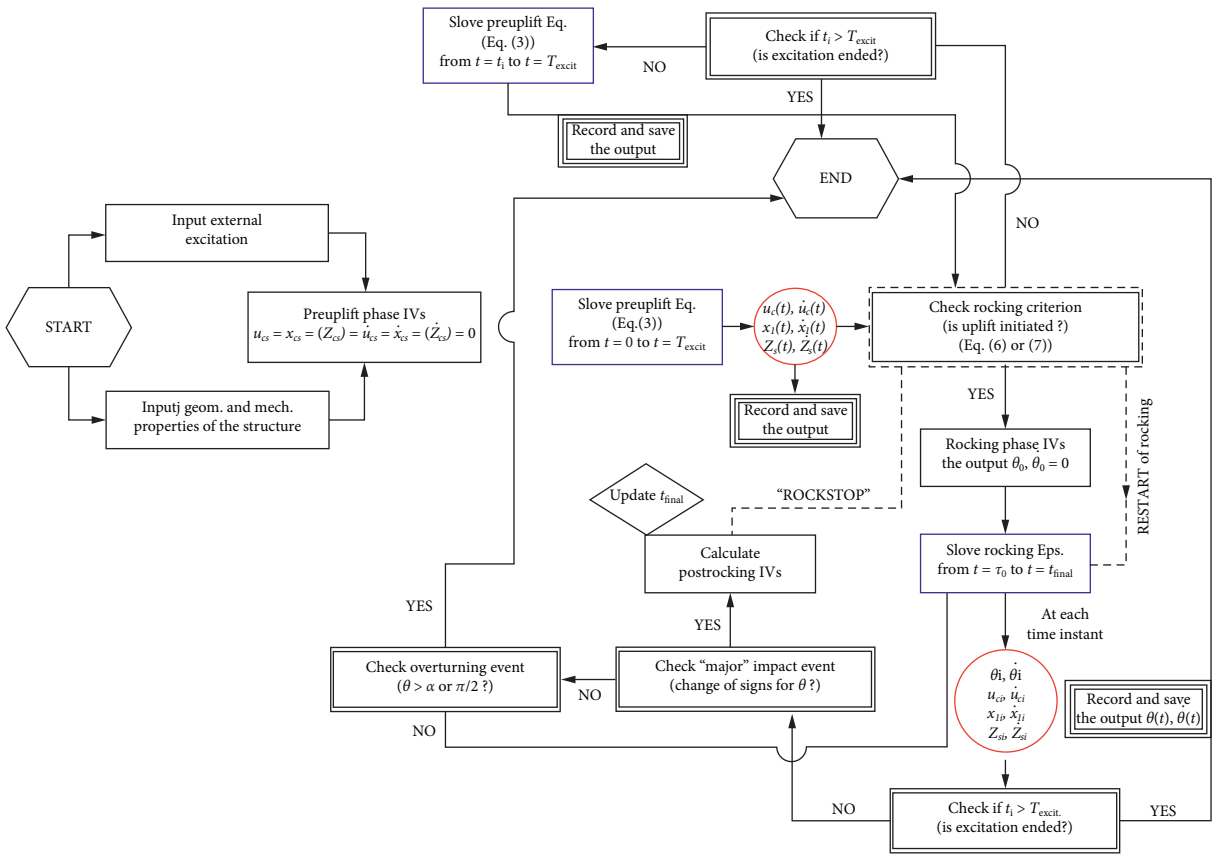

Figure 7: Flowchart of the analysis procedure implemented in MATLAB.

To produce solutions with enough accuracy, a local error (ε) is estimated at each time step by the solver which must be less than or equal to an acceptable error (ε_a) as follows:

$$\varepsilon \leq \varepsilon_a = \max[\text{RelTol} \times \text{abs}(y(i)), \text{AbsTol}(i)]. \quad (22)$$

In this equation, RelTol is a scale of the error relative to the size of each solution component and roughly controls the number of correct digits in all solution components. Also, AbsTol is a limit quantity below which the value of each component is "unimportant." This tolerance specifically determines the accuracy when a solution component approaches zero [41], as in the impact events of rocking structures where θ and $\dot{\theta}$ reaches zero.

Accordingly, the aforementioned acceptable error is used to control the time-step size (dt) used in the integration process. This, again, should be carefully controlled during the impact events. On the other hand, since the EOMs in the rocking phase of motion are nonlinear and mathematically "stiff," the maximum time-step size should be limited so that the solver does not increase the time step too much and step over the impact events or other critical events.

In addition to the above arguments, relative tolerances, absolute tolerances, and the maximum step size used in this study were determined based on a sensitivity analysis of the results. Thus, the relative and absolute tolerances were selected as small as 10-11 and 10–12, respectively, which the former corresponds to a same rate of accuracy. Finally, considering the smallest vibration period of the system components, the maximum time-step was set to 10–3.

In addition to the numerical stiffness of the EOMs, the solver configurations described above resulted in time-consuming calculations. Thus, another modification was also adopted. It was observed that over 90% of the time needed for running the analysis procedure of a sample structure is consumed in the rocking phase of motion and for detecting the "major" impact events. The term "major" is described as follows: it is observed that a major impact is followed by a combination of multi serial microimpacts located at very small time intervals and also negligible postimpact response amplitudes (see Section 5.1). Generally, solution of the rocking EOMs is done over the time intervals of t_{uplift} (uplift time instant) to t_{final}, which is the time instant for a major impact. From this instant onward, there is not a significant rocking motion for some time. Thus, if t_{final} is determined, neglecting the effect of other microimpacts, whose calculation is futile and time-consuming, the rocking phase can be stopped sooner and the time needed for running the script reduces significantly. For this purpose, if the time intervals between the microimpact events and their corresponding postimpact responses simultaneously become too small (<10–8), it is concluded that the rocking phase was terminated by a "major" impact. While these conditions are not verified for most of the analyses on C1, the solution process of which is not very time-consuming, this strategy is more useful for C2. The aforementioned

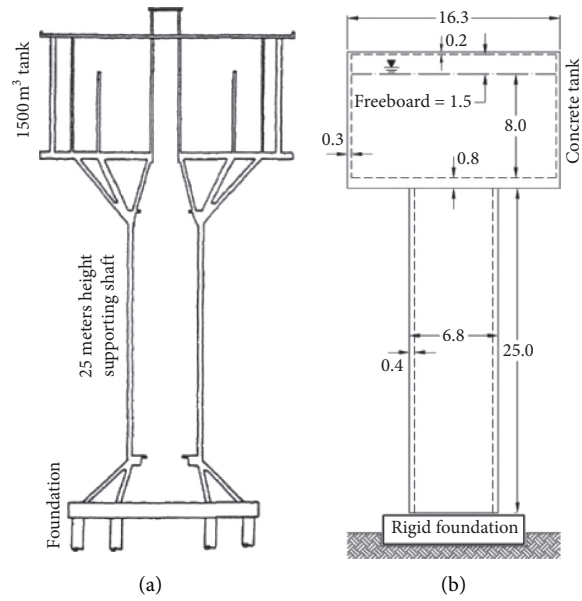

Figure 8: (a) Schematic section of water tower No. 1 located in Rasht, north of Iran, which collapsed during Manjil, 1990, earthquake, and (b) dimensions of the simplified concrete model

numerical procedure is implemented in an original MATLAB script, the flowchart of which is illustrated in Figure 7.

4. Description of the Study Group

A study group including 18 structures with various geometrical and structural properties as the "prototypes" is selected in this paper so that the extensibility of the analyses can be verified. The base geometry of the prototypes was selected in accordance with a real structure, namely, water tower No. 1 which was located in Rasht, north of Iran, and collapsed during 1990 Manjil earthquake [43]. A schematic section of this structure is shown in Figure 8(a). Dimensions of the simplified model studied here with a concrete tank is shown in Figure 8(b).

Assuming the basic 25-meter-high shaft as a mid-rise structure, two other heights, 15 (m) for low-rise and 35 (m) for high-rise structures, were also chosen to include the effect of shaft height in the study. Moreover, 3 different tank filling levels (full, half, and empty) are also selected to study the effect of liquid heights on the flexibility and convective components of the response. Both the shaft and the tank of all prototypes are presumed to be symmetric cylindrical shell structures. Finally, assuming (H_L/R) equals 1 and the wall thickness to radius ratio (t/R) equals 0.04 for the concrete tank, characteristics of the equivalent models are calculated per the analytical analogy of Figure 4 and Section 2.2 and given in Table 1.

5. Results Description for a Sample Structure

5.1. Free Vibration Analysis. One of the introduced prototypes with a 25-meters high shaft and a concrete tank in full case (25-1-CONC) is chosen as the sample structure. The normalized free vibration response of this sample structure to a given initial tilt angle of $\theta_0 = 0.0065\,(\text{rad})$ is shown for the first and second cases of RI in Figure 9. These results are also compared to those of a "similar" fixed-base structure (with subscript "mFB") which is analyzed with an initial displacement of $\theta_0 H_S$ assigned at the end of its shaft. Portions of the flexibility response in Figure 9 (blue boxes) which experience high-frequency vibrations are shown separately in zoomed-in views of Figure 10.

It is worth to note that in these analyses, the fixed-base damping ratio of the shaft and the tank wall is taken to be 0.015 while the damping ratio of the convective component is equal to 0.005. These values are proposed mainly for a structure/tank which is assumed to remain elastic during a seismic excitation [10, 44]. Accordingly, the following remarks are drawn:

(a) Convective response: between every two consecutive impacts, the system components except convective enter a state of motion, i.e., "uplifted state," which experiences higher frequency elastic vibrations and damping ratio. This is a similar state reported by other researchers for structures with foundation uplift [4] or deformable rocking structures [10]. However, the response of the convective component does not follow this state and frequency decreases in both RI cases. For instance, linearizing equation (15) and omitting the term of base excitation gives

$$\ddot{u}_C + \left(\omega_C^2 - \dot{\theta}^2\right)\left(u_C - z_S\right) + 2\xi_C\omega_C\left[\dot{u}_C - \left(\dot{z}_S + H_m\dot{\theta}\right)\right] = 0. \tag{23}$$

Hence, from equation (23), the uplifted frequency, $\omega_{C,\text{up}}$, and uplifted damping ratio, $\xi_{C,\text{up}}$, of the convective component are approximately as follows:

Table 1: The characteristics of the equivalent simplified liquid-tank system calculated for the sample structures with various filling levels.

System parameters		Analytical values		
		Full case	Half-full case	Empty case
Convective component	m_C (ton)	667.0	513.2	—
	H_{Cb} (m)*	6.2	6.1	—
	K_C (kN/m)	1463.1	866.3	—
	C_C (kN.s/m)	9.9	6.7	—
Flexibility component	m_1(ton)	1060.0	524.6	—
	H_{1b}(m)*	5.8	5.4	—
	K_1 (kN/m)	5.9×10^7	1.1×10^8	—
Impulsive component	m_0 (ton)	181.3	76.8	358.1+
	I_G^0 (ton.m2)	7.8×10^3	7.9×10^3	1.4×10^4
	H_{0b} (m)*	3.8	3.8	4.75++

*The subscript "b" indicates that the equivalent heights are calculated with the inclusion of the effect of the pressure variation on the tank floor. +Mass of the tank wall. ++C.G. height of the tank wall.

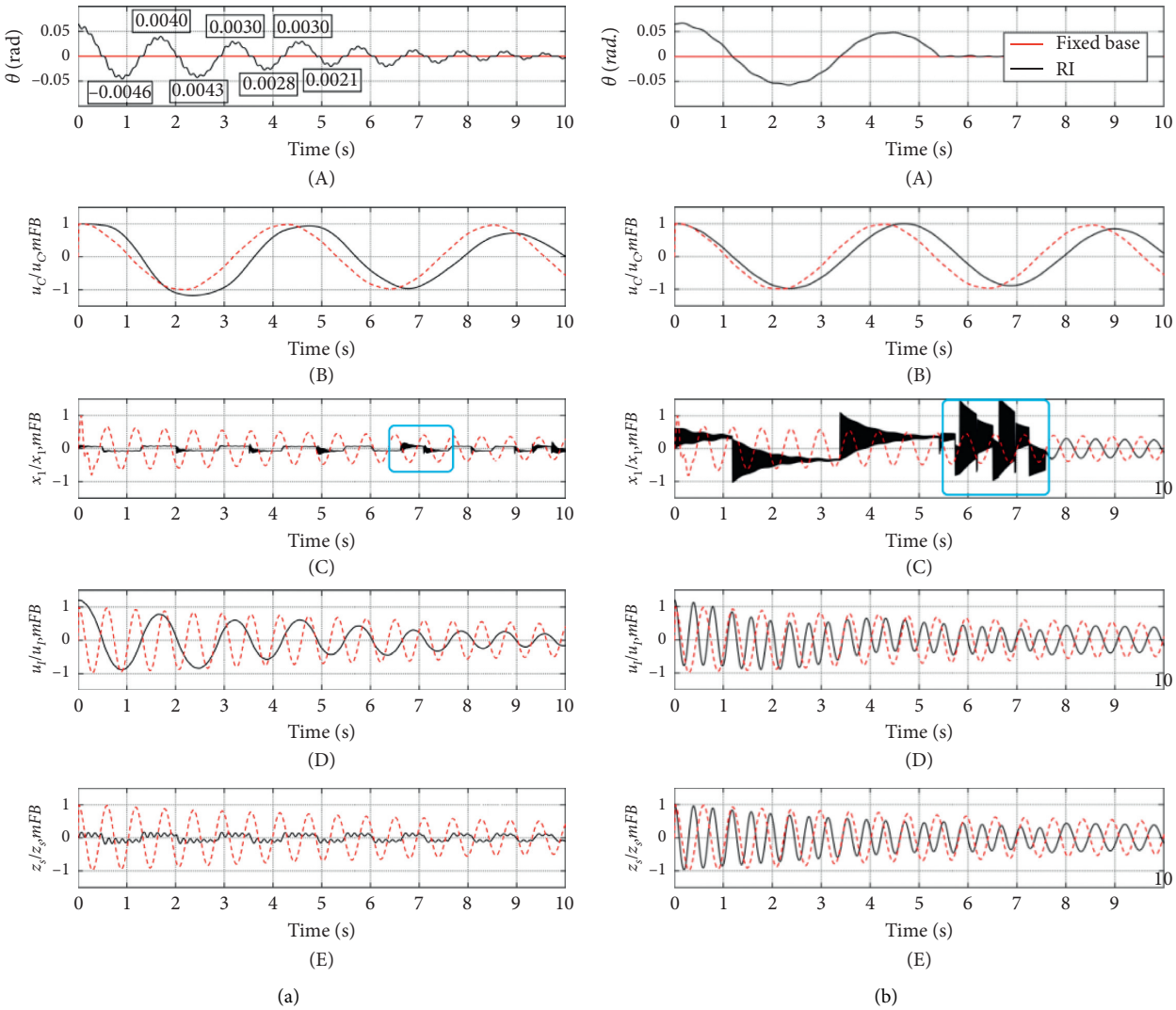

Figure 9: Normalized time histories of free (A) rocking, (B) convective, (C) wall flexibility, (D) impulsive, and (E) shaft top end responses for a sample structure with "first case of RI-C1" (a) and "second case of RI-C2" (b) to an initial tilt angle.

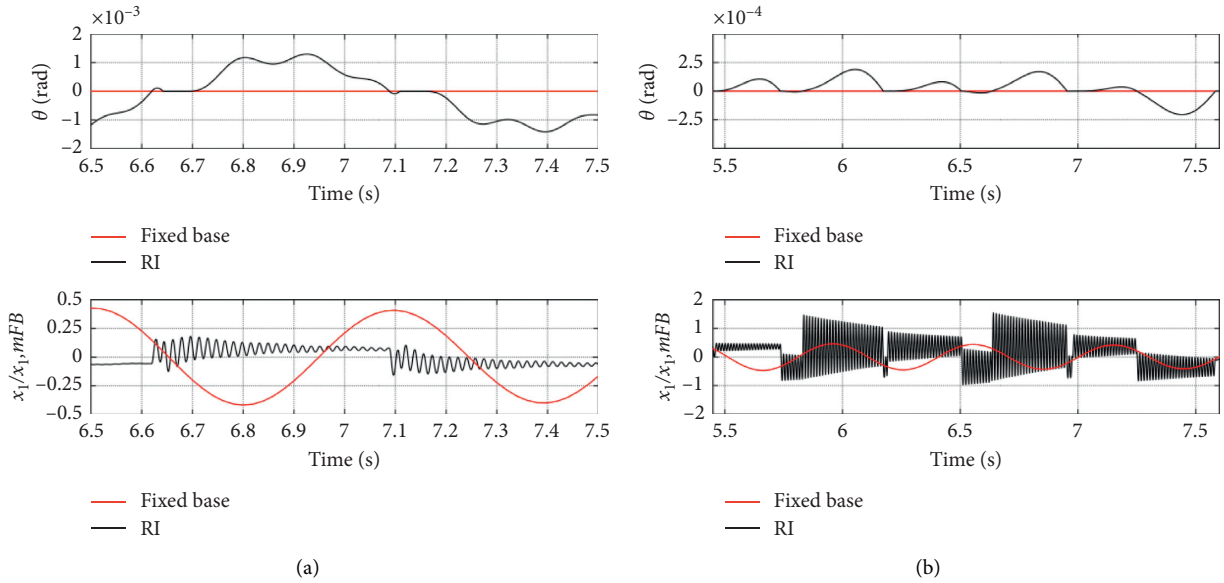

Figure 10: Zoomed-in views of the high-frequency vibrations of flexibility components in Figure 9 for the system with C1 (a) and C2 (b).

$$\omega_{C,\mathrm{up}} = \sqrt{\omega_C^2 - \dot{\theta}^2}, \tag{24}$$

$$\xi_{C,\mathrm{up}} \approx \xi_C \left(\frac{\omega_C}{\sqrt{\omega_C^2 - \dot{\theta}^2}} \right), \tag{25}$$

where by increasing $\dot{\theta}$, the uplifted frequency decreases but the damping ratio increases.

(b) Wall flexibility response: it has been reported experimentally [12] that stiffer structures experience stronger vibrations after each impact. This explains the high-frequency vibrations of the wall flexibility components illustrated in Figure 10. But, from another point of view, wall flexibility component is so stiff ($\omega_{\mathrm{fund}} > 200$) that its motion is constrained with the shaft motion, i.e., moving "in phase" with the shaft and oscillating with a close amplitude ratio of the shaft:

$$\left(\frac{x_1}{x_{1,m\mathrm{FB}}} \right) \approx \left(\frac{z_S}{z_{S,m\mathrm{FB}}} \right). \tag{26}$$

Hence, even after uplift, oscillation amplitude of the wall flexibility component in the first case of RI (C1) is reduced with almost the same ratio of the shaft. But similar high-frequency vibrations (Figure 10(a)) persist because of its even larger stiffness ($\omega_{1,\mathrm{up}} > \omega_{1,\mathrm{fund}}$). This is not, however, the case for the second case (C2). Applying the RI only to the tank does not reduce the shaft response as that of C1. Thus, the wall flexibility component in C2 is affected more by the impacts and experiences stronger frequency vibrations (Figure 10(b)). This results in even larger deformations than the fixed-base structure.

(c) Impulsive and shaft responses: the impulsive response in C1, which is also studied as the tank C.G., is dominated by the rocking response of the whole structure and increases up to 12% of that of the fixed-base system. But, in C2, it is a superposition of the shaft and rocking responses with more domination from the shaft. Thus, it does not change notably compared to the fixed-base system.

(d) Interaction of convective and rocking response: in structures with C1, the interaction of convective response affects the history of rocking response (θ), number of impacts, and the ratio of dissipated energy. For instance, after the second impact at 1.4 (s), while the third peak θ tends to decrease, the convective response acts in the opposite direction, and hence the peak decreases more. In this case, the convective and rocking responses acted "out of phase." But, the opposite happens after the third impact at 2.1 (s). While it is expected that θ decreases because of the new impact and its energy dissipation mechanism, being the convective component, "in phase" of θ results in a larger absolute peak (0.0043 (rad)) in comparison to the previous peak value (0.0040 (rad)). Although this continues for the rest of the motion, the rocking response keeps decreasing in an irregular pattern (Figure 11(a)) that differs from other structures with RI. Comparison of these results with those of a similar RI system with equivalent mass and geometry but without the "interacting" effect of the convective component is shown in Figure 11(a). As illustrated for the sample structure, existence of the convective component increases the number of impacts and also the amount of dissipated energy over the same time duration (Figure 11(b)). This also shows that the convective component can be proposed as an "additional" energy dissipation

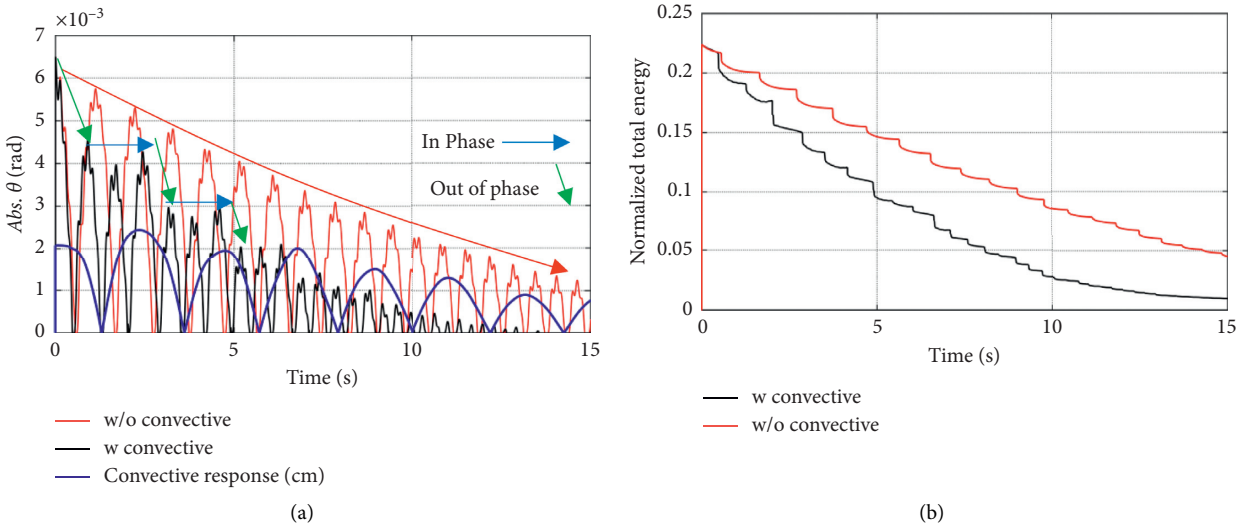

FIGURE 11: Time history of absolute rocking response (b) and normalized total energy (a) of the system with C1: "with" and "without" the convective component.

and damping mechanism in structures with free rocking motion, which are generally considered as systems with very low radiation damping [45, 46], i.e., from the radiated energy on each impact. Thus, the convective component plays a notable role in the dynamic analysis of liquid tanks with RI.

(e) Energy dissipation in C2: as discussed in [45, 46], squat rocking structures (H/B ≤ 1) show larger radiation damping. Hence, after the third impact in C2, the rocking response damps out greatly, approximately becoming zero. However, it is then followed by a series of microimpact-uplift transitions as shown in Figure 10 (right top) which is originally a numerical instability issue emerging from the procedure described in Section 3. Nevertheless, this phenomenon has resulted resulted in resonance and high-frequency vibrations of the flexibility component as described in (c).

5.2. Seismic Response History Analysis (SRHA)

5.2.1. Deformation and Rotation-Based Responses. The results of seismic response history analyses of the same sample structure under the action of 1990 Manjil earthquake recorded at Tonekabon station (R#4-PEER RSN 1640 [47]) (Figure 12) are presented in this section. As shown later (Section 6.1), this was a far-field event with a weak vertical component and higher spectral powers in the frequency ranges of 1.2–1.5 (Hz). Namely, the lateral displacement and hydrodynamic pressure demands of the convective (u_C and P_C), flexibility (x_1 and P_1), and impulsive (u_I and P_I) components of the liquid-tank system in addition to the deformation response of the shaft (z_S) are obtained and normalized to the maximum responses of the similar fixed-base structure (mFB). Deformation responses of the sample structure with "first case of RI" (C1-isolation at the base) and "second case of RI" (C2-isolation under the tank) are, respectively, shown in Figure 13.

As discussed in free vibration analysis (FVA), under the action of 1990 Manjil earthquake, same "uplifted states" are observed. This is specifically the case for the shaft flexural response in C1. Moreover, while the oscillation amplitude of the tank wall decreases up to 40% of the fixed-base system with C1, it increases up to 20% for C2. Similarly, other remarks explained in FVA section hold for the response of other components. It is noteworthy that the seismic rocking motion of C2 is a serial pulse-like motion with rocking responses as low as 0.0004 (rad.) (Figure 13(a)). Firstly, it seems that these finite uplifts make no difference in the seismic response, comparing to a fixed-base tank. But the succession of these finite uplifts simulates an uplifted state which results in lower deformation responses of the tank and shaft (Figures 13(b) (D) and (E)). But, the convective response of the system is not affected by this phenomenon due to small values of $\dot{\theta}$ (equation (24)). Nevertheless, response of the shaft in C2 acts more like the slide-isolated systems [26, 28] with no considerable change in oscillation frequency or phase.

5.2.2. Acceleration-Based Responses. For response assessment of rocking structures, the effect of RI is often studied on the rotational [2–8] or displacement demands [9–11, 16, 48] of the system. However, in liquid storage tanks, acceleration is also a crucial response component for determining force and pressure demands. The lateral hydrodynamic pressure demand P_n induced by each component of the liquid-tank system is calculated by

$$P_n = \ddot{u}_n^{\text{total}} m_n, \tag{27}$$

where m_n is the mass of the corresponding component (n = C, x, I) and $\ddot{u}_n^{\text{total}}$ is the "total" acceleration response which is described by

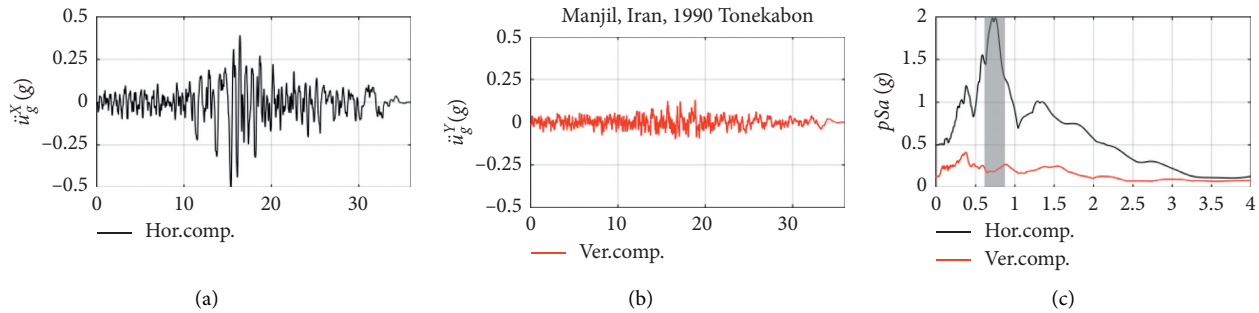

FIGURE 12: 1990 Manjil earthquake recorded at Tonekabon station: (a) horizontal component, (b) vertical component, and (c) the pseudoacceleration spectra where ranges of period with higher horizontal spectral power are shown in grey.

$$\ddot{u}_n^{\text{total}} = R_n\ddot{\theta}\cos\alpha_n + R_n\dot{\theta}^2\sin\alpha_n + \ddot{z}_n, \tag{28}$$

for various components. Sum of these hydrodynamic forces gives the total shear at the base of the tank wall.

Accordingly, time histories of the normalized hydrodynamic forces acting on the tank wall of this prototype are plotted in Figure 14. As defined by equation (27), it can be shown that the same discussions for deformation responses, such as uplifted states, govern acceleration responses of the system too. Hence, the same changes are observed in acceleration responses and hydrodynamic force histories of the liquid-tank system. However, $\ddot{u}_n^{\text{total}}$ for flexibility and impulsive components is also affected by the sudden changes in the signs and values of angular/translational velocity components $(\dot{\theta}, \dot{z}_n)$ due to impact transitions (equations (19)–(21)). The effect of close/serial impacts is the other parameter acting on the acceleration responses; specifically look at response of the structure with C2 (Figure 13(a)) or the beginning part of the response of the one with C1 (Figure 13(a)). The larger are the time intervals between the two consecutive impacts; the structure has more time to damp out the vibrations and to reduce the acceleration responses. Thus, it can be concluded that the first case of RI (C1) generally decreases the acceleration responses of the structure, while C2 holds the opposite. Nevertheless, in neither of the RI cases, the acceleration response of the convective component $(\ddot{u}_C^t)$ is not affected by the impact transitions, as discussed in the next section.

Superposition of all hydrodynamic forces of the liquid-tank system gives the "tank-base" shear force history (V_{Tank}). Impulsive force demands of tank roof and floor are also added to this force. Then, by adding this shear force to the shear force induced by shaft vibrations, total base shear (V_{Total}) (shaft-base) is calculated (Figure 15). As shown, (V_{Tank}) and (V_{Total}) of the structure with RI are reduced more in C1 (10%) than C2 (50%). Moreover, studying (V_{Total}), while the rocking shaft in C1 decreases (V_{Tank}) by almost 4% more, the fixed-base shaft in C2 increases (V_{Tank}) by almost the same amount. It should be noted that although hydrodynamic forces of flexibility and impulsive components in both RI cases are separately larger than those of the fixed-base structure in some timespans (Figure 14), but the components act in the opposite direction of each other during these timespans. Hence, the summation, i.e., (V_{Tank}), is lower than the fixed-base structure.

5.2.3. Sloshing and Wave Oscillations. Finally, the fluid inside storage tank sloshes during an earthquake event, and thus a freeboard allowance is needed. For this purpose, maximum wave oscillation Δ_{wave} caused by earthquake acceleration and the required freeboard allowance is defined and calculated as the vertical displacement of the fluid surface by

$$\Delta_{\text{wave}} = \left(\frac{D}{2}\right)(A_{\text{tot}}/g), \tag{29}$$

where D is inside diameter of the tank, A_{tot} is the total acceleration of the convective component $(\ddot{u}_C^t = \ddot{u}_C + \ddot{u}_g^X)$ of the liquid-tank system, and g is the gravitational acceleration.

Time histories of wave oscillation of the sample structure are normalized to the 1.5 m freeboard provided for the similar fixed-base structure (Figure 8) and shown in Figure 16. As discussed previously (equation (24)), seismic oscillation frequency of the convective component decreases in the system with both RI cases.

Additionally, interacting effect between rocking and convective motions in C1, as discussed in the FVA section, leads to slightly larger convective acceleration response. Thus, larger wave vibrations are obtained. However, the sample structure with C2 does not experience any notable change in acceleration response under the action of 1990 Manjil earthquake (R#4). It is shown in the next section that freeboard requirements of rocking elevated tanks are needed to be revisited.

6. Parametric Analysis of the Response under Multiple Hazards

In previous sections, the analytical abilities of the developed model are exemplified. Hereafter, the objective of the study is to obtain basic information on the applicability of the RI as a seismic response upgrade technique for elevated tanks. Various parameters were included in the analysis based on the various properties of the study group introduced in Section 4.

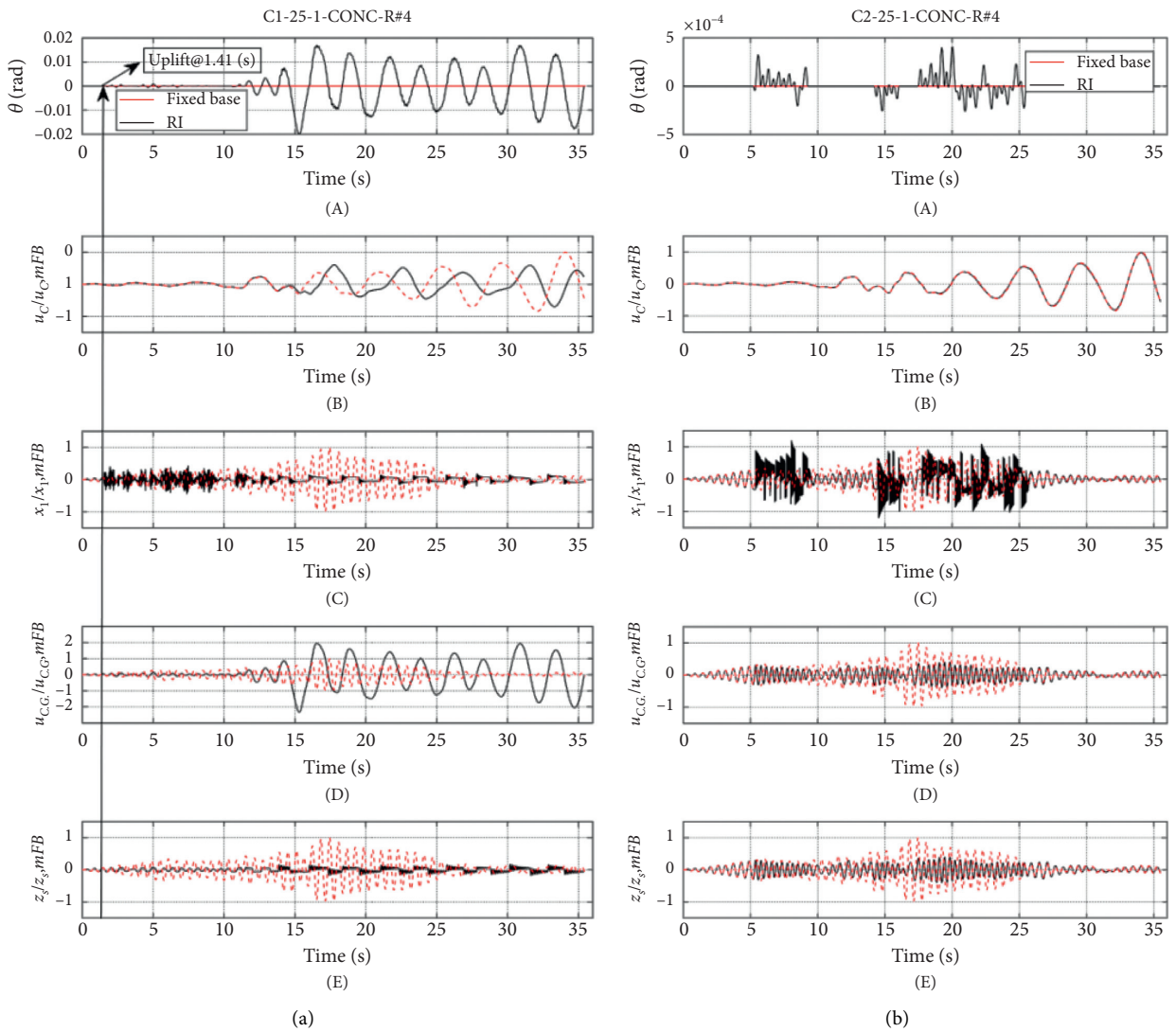

FIGURE 13: Normalized time histories of (A) rocking, (B) convective, (C) flexibility, (D) impulsive, and (E) shaft top end deformation responses for the structure with C1 (a) and with C2 (b).

Additionally, considering that the system with RI may also be vulnerable to other lateral loadings, the effects of wind loads are also studied in this section. The wind loads were assumed to act statically in two combinations: (1) independently before or after the seismic excitation and (2) simultaneously with the seismic excitation. In the latter case, it is assumed that the wind duration was long enough [49] to happen concurrently with the maximum ground accelerations. It is worth to note that in some seismic prone zones, such as the city of Manjil, north of Iran, average wind speed is always so high [50]. Thus, the second combination could be the worst scenario of lateral loads acting on an essential structure such as an elevated water tank.

6.1. Seismic Excitations. The introduced study group (Section 4) was excited by an ensemble of 3 pairs of recorded far-field ground motions with properties shown in Table 2. Each pair includes the horizontal and vertical components of the event (Figure 17). The accelerograms are recorded mostly on firm site (site class C) and are chosen from the PEER NGA-West 2 database [47]. The records were scaled to the MCER response spectrum of ASCE 7-16 [37] for the high-seismicity zones, i.e., SD1 = 0.66 (g) and SDS = 1.26 (g).

In free rocking structures such as the system studied here, the oscillation frequencies change with the rocking amplitudes and there are no unique fundamental frequencies. However, as discussed in Section 5.1, the system can be studied over a range of frequencies close to the frequencies of the similar fixed-base system. Thus, the period range for scaling has an upper bound corresponding to the "first convective mode" and a lower bound that corresponds to the first vibration mode of an empty structure, i.e., almost 0.15 (s). The records were scaled such that the average spectrum of all horizontal components does not fall below 90% of the target spectrum for any period within the mentioned range (Figure 17(c)). Accordingly, the spectral properties of the ensemble were chosen so that each pair excites various

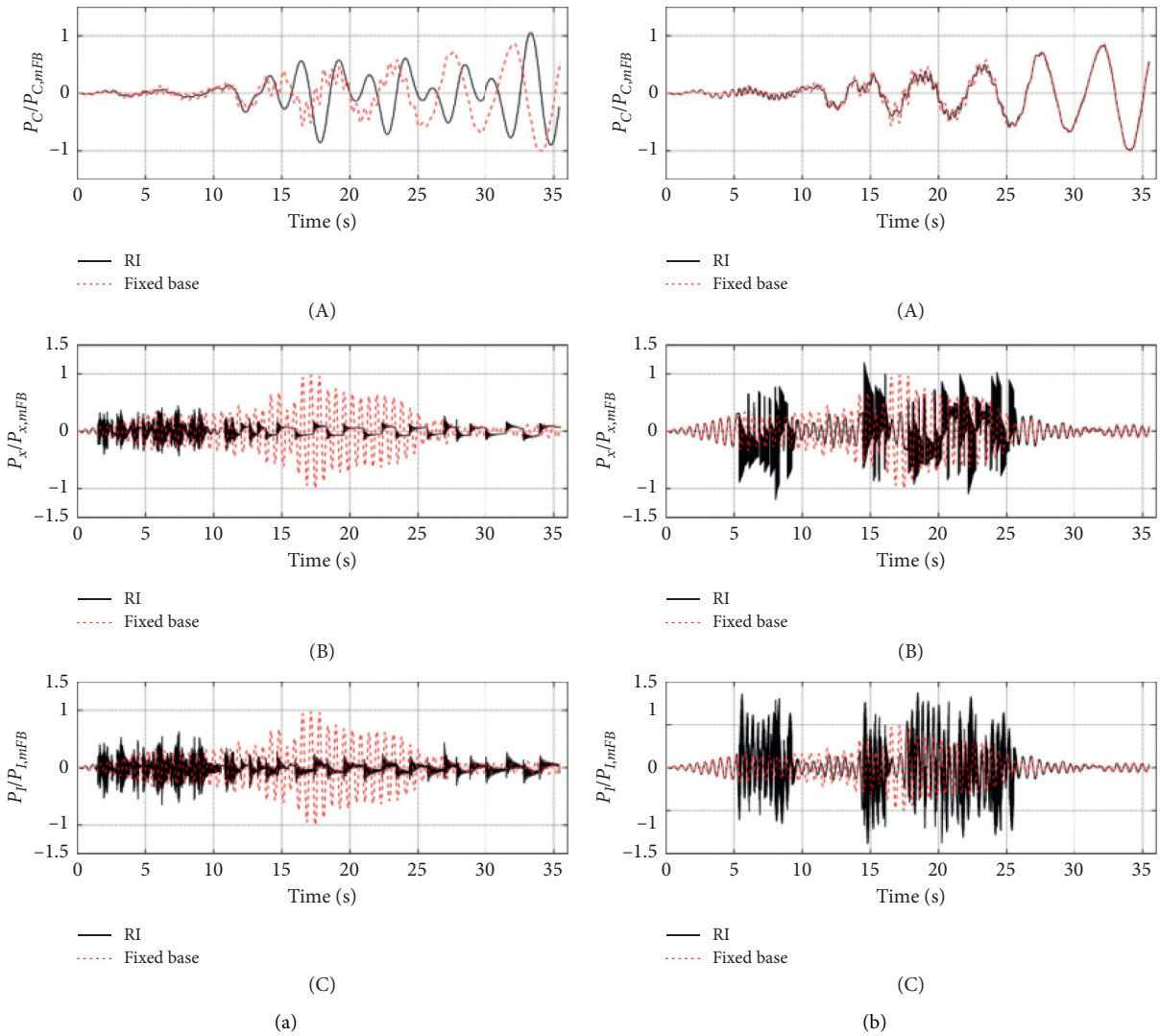

FIGURE 14: Normalized time histories of the distributed hydrodynamic forces induced by (A) convective, (B) flexibility, and (C) impulsive components for the structure with C1 (a) and C2 (b).

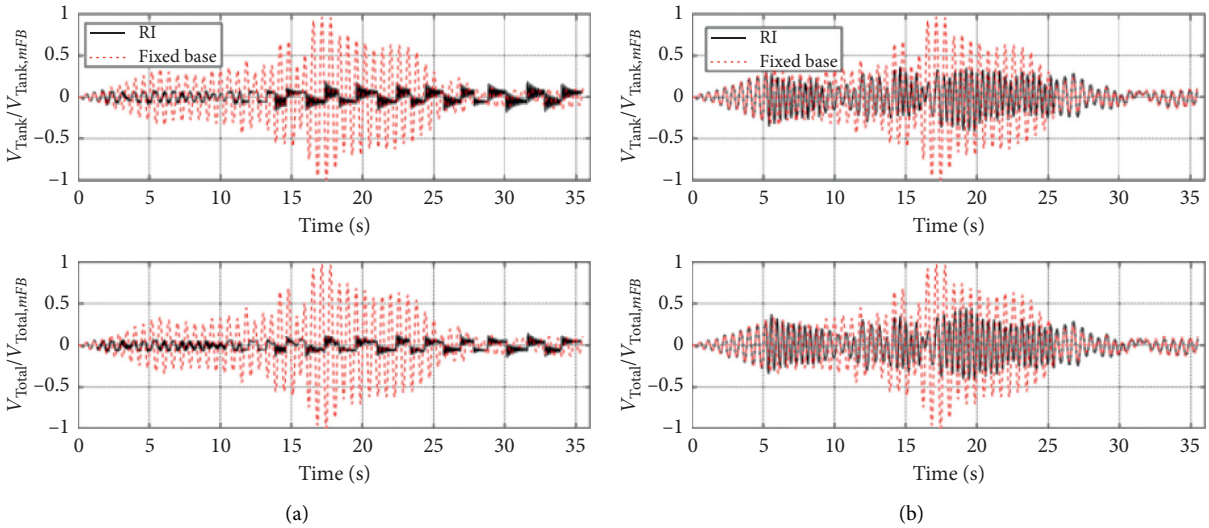

FIGURE 15: Normalized tank-base (V_{Tank}) (top) and shaft-base (V_{Total}) (bottom) shear forces for the sample structure with C1 (a)(left) and C2 (b).

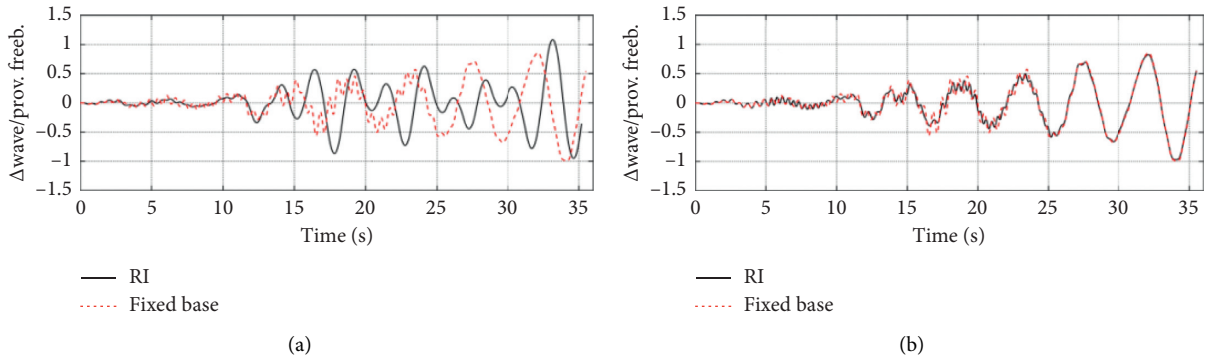

Figure 16: Normalized tank-base (top) and shaft-base (bottom) shear forces for the sample structure with C1 (a) and C2 (b).

Table 2: Properties of the recorded ground motions used for the seismic response analysis.

No.	Event	Year	Station	PEER RSN	M_W	RDF* (Hz)	VCS**	PGA_{scaled} (g) ***
1	Manjil	1990	Tonekabon	1640	7.4	1.2–1.5	Low	0.53
2	Manjil	1990	Abhar	1634	7.4	0.27–0.32 1.5–4.0	Low	0.43
3	Landers	1992	Yermo Fire Station	900	7.3	0.6–5.0	High	0.61

*Record dominant frequencies: the range of frequencies with higher spectral power. **Vertical component significance: "high" for records with strong vertical component and vice versa. ***PGA of the scaled horizontal component (g).

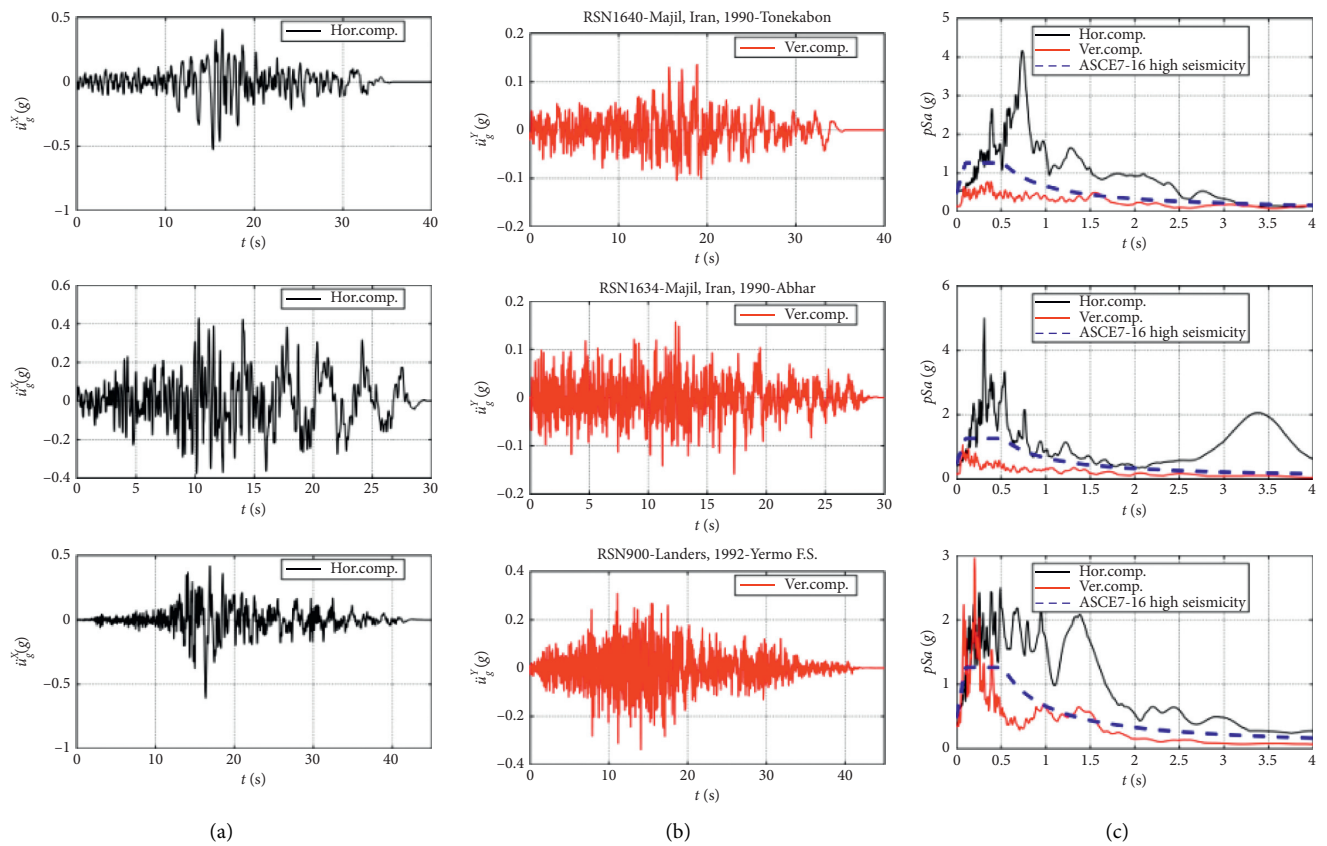

Figure 17: Ensemble of the scaled seismic records used as the base excitations: (a) (left) horizontal components, (b) (middle) vertical components and (c) (right) comparison of pseudo-acceleration spectra with the target spectrum.

Table 3: Design wind load parameters of the circular shaft and tank.

Risk Category	V (m/s)	Exposure Category	Enclosure Classification	K_d	K_{zt}	K_e	G	K_z ($\alpha = 0.9$, $z_g = 274$)	C_f
IV	45.0	C	Partially open	1.0	1.0	1.0	0.85 (rigid structure)	$2.01\,(4.6/z_g)^{\frac{2}{\alpha}}$, $z \le 4.6\,(m)$ $2.01\,(z/z_g)^{\frac{2}{\alpha}}$, $4.6 < z < z_g$	0.7

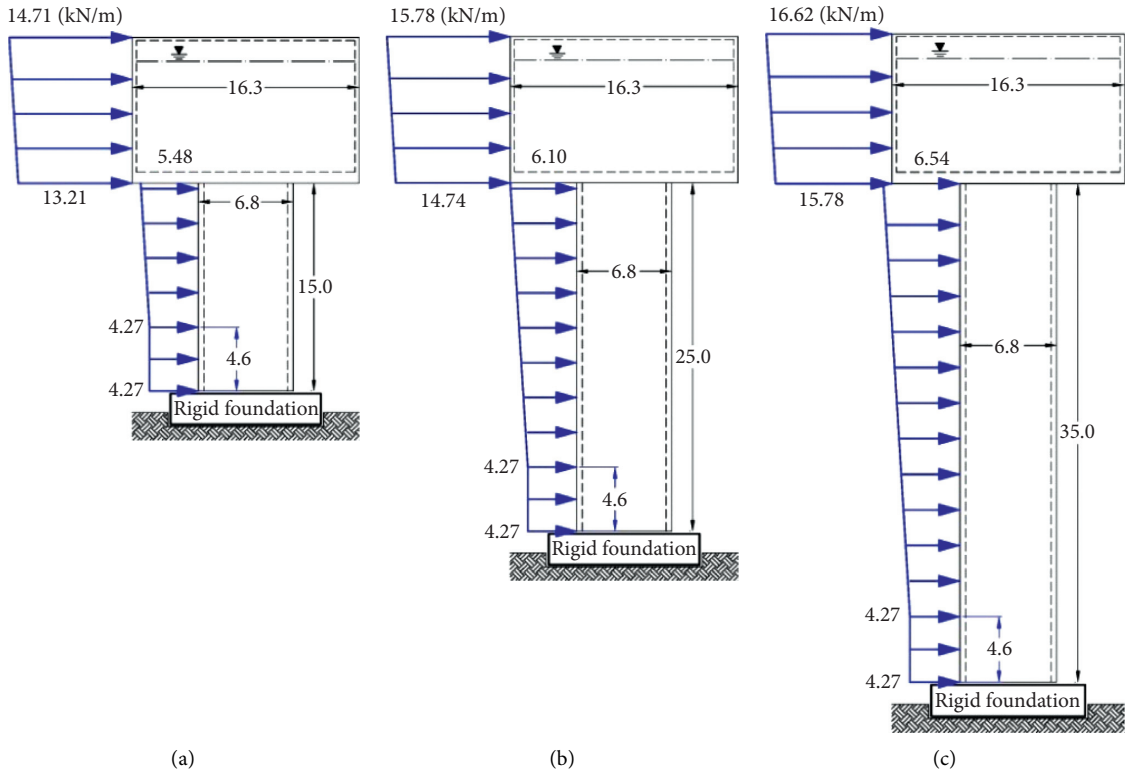

Figure 18: Distributions of design wind load in the height of the prototypes (dimensions are in meters). (a) 15-meter-high shaft. (b) 25-meter-high shaft. (c) 35-meter-high shaft.

ranges of frequency. The third pair (RSN900) was specifically chosen to study the effect of vertical component.

6.2. Details of the Wind Load. The wind loads are evaluated based on the requirements of ASCE 7 for Risk Category IV structures [37]. The basic wind speed for determination of the design loads was selected to be 45 (m/s) which corresponds to wind hazard zones with highest gust speed in Iran [51], such as Manjil. Wind load parameters are summarized in Table 3. Distributions of design wind loads in the height of the prototypes are also shown in Figure 18.

6.3. Dimensionless Parameters. Numerous properties of the selected prototype structures and also a high number of dominant parameters make dimensionless response assessment difficult. However, the responses can be normalized to those of a fixed-base structure with similar geometrical and engineering properties. Thus, interpretation of the results and lateral performance upgrade of the prototypes become more practical. For this purpose, 5 dimensionless parameters (λ_is for deformation and $\Pi_i s$ for force/moment responses), each as a ratio of the maximum responses, were defined as follows:

$$\lambda_\Delta = \left(\frac{\Delta^{\max}_{\text{wave,RI}}}{\text{Prov.Freeb.for FB}}\right),$$

$$\lambda_{C.G.} = \left(\frac{u^{\max}_{0,\text{RI}}}{u^{\max}_{0,\text{FB}}}\right),$$

$$\lambda_S = \left(\frac{z^{\max}_{S,\text{RI}}}{z^{\max}_{S,\text{FB}}}\right), \tag{30}$$

$$\Pi_V = \left(\frac{V^{\max}_{\text{base,RI}}}{V^{\max}_{\text{base,FB}}}\right),$$

$$\Pi_M = \left(\frac{M^{\max}_{\text{base,RI}}}{M^{\max}_{\text{base,FB}}}\right),$$

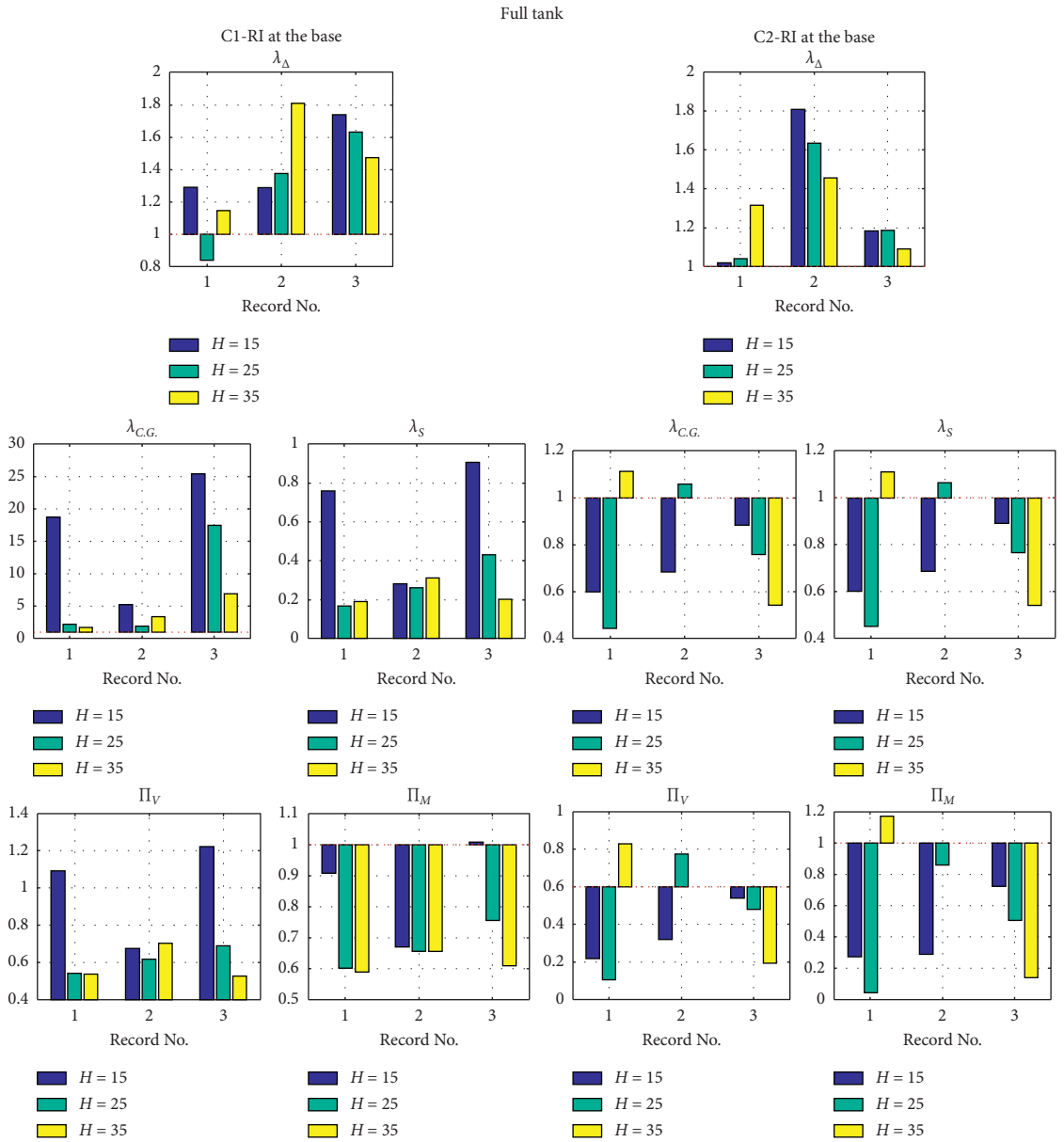

Figure 19: Performance of the prototype structures with "full tank" and various "shaft heights" (15, 25, and 35 (m)).

where the parameters with subscript "FB" corresponds to the similar "fixed-base" structure with its provided freeboard assumed to be 1.5 (m). Moreover, u_0 is the horizontal displacement of the impulsive mass (m0 in Figure 4) which approximately estimates the displacement at the C.G. of the liquid-tank system. It is worth to note that the practical ratios of importance factor to the response modification factor (I/R_u) for the fixed-base elevated storage tanks are almost equal or smaller than 1 [37, 44]. Thus, the aforementioned parameters provided comparable information about design applicability and effectiveness of RI for response mitigation of elevated liquid storage tanks. Using these parameters, "three" main performance categories of the systems were evaluated: (1) operational ($\lambda_\Delta, \lambda_{C.G}$), (2) structural ($\lambda_S$), and (3) force performances (Π_V, Π_M).

In the following illustrations (Figures 19–22), the dimensionless parameters were obtained and compared for various RI cases, seismic excitations, shaft heights, and tank filling levels. Accordingly, two load combinations including (1) independent seismic hazard and (2) concurrent seismic and wind hazards ($S + W$), were distinguished in these illustrations. Moreover, the red dashed baseline in some graphs showed the cases that their responses went beyond those of a similar fixed-base structure. Specifically for force/moment responses, this demonstrates the downgrade of the performance.

7. Discussion of the Results and Performances

In this section, the effect of various parameters on the (1) operational, (2) structural, and (3) force performances of the proposed RI systems is discussed.

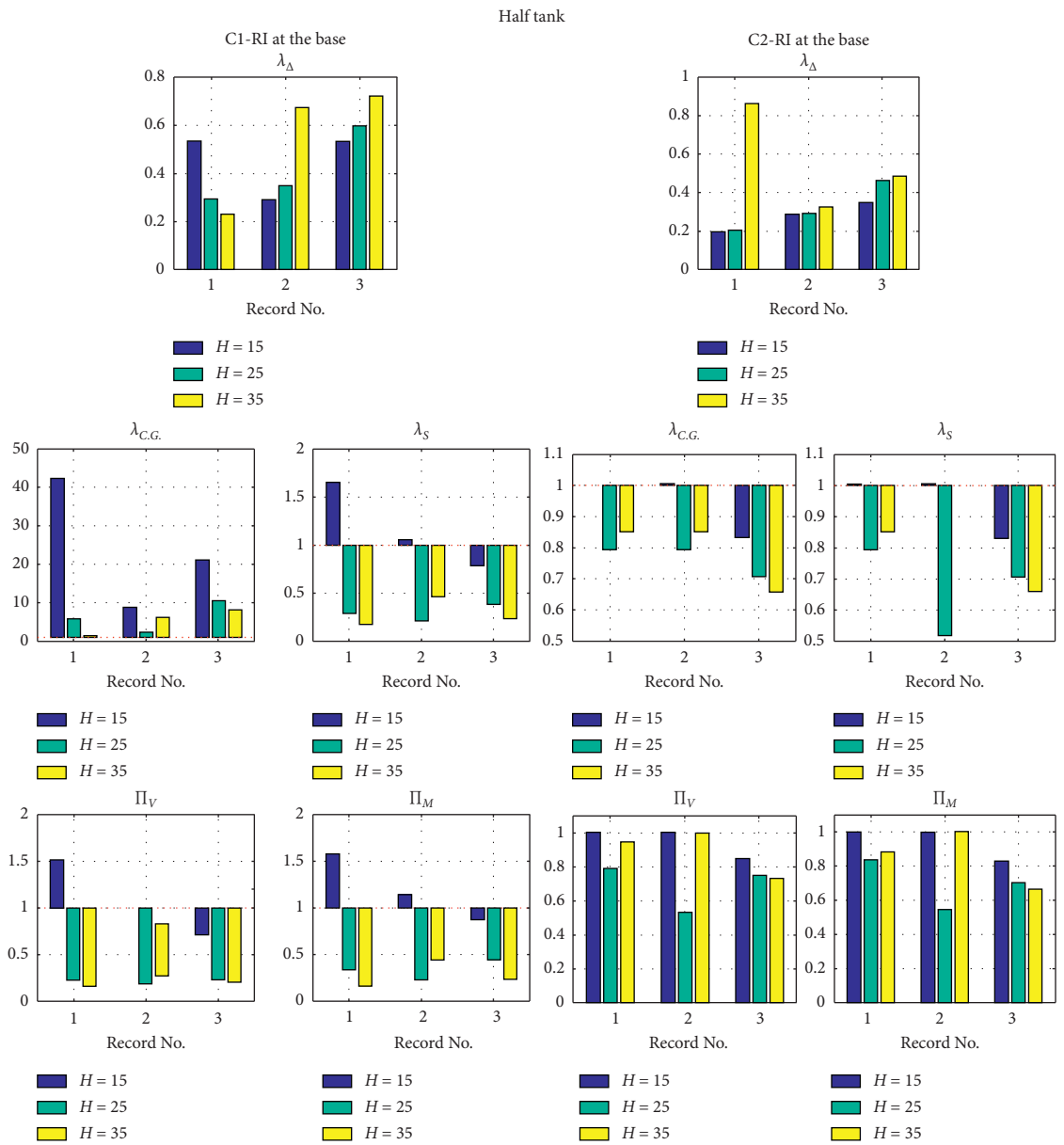

Figure 20: Performance of the prototype structures with "half tank" and various "shaft heights" (15, 25, and 35 (m)).

7.1. The Effect of RI Cases

(1) The convective response and wave oscillations, as main "operational" components, are directly affected by RI. The wave oscillations are increased by both large rocking responses (θ) and also amplified convective accelerations ($\ddot{u}_C$) at the level of the tank. The other operational component is the tank C.G. displacement (u_0) which is mainly affected by rocking response of the whole system.

As discussed in Section 5, the first RI case (C1: RI at the base) developed larger rocking responses (?) than C2. Thus, the prototypes with C1 experienced larger C.G. displacements than those with C2 (Figure 19, 20, 22 (middle), and 21 (top)). Under the action of the considered ensemble of the seismic motion, the prototypes with C2 showed almost no advantage over the fixed-base structures. Nevertheless, the prototypes with C1 underwent responses 10 to 50 times larger than those of the fixed-base structures. This corresponded to rocking responses about 0.1 (rad), which was also in a safe margin of overturning, i.e., $\theta_{cr} \approx 0.2$ (Figure 22).

Unlike the C.G. displacements, the convective performances and freeboard allowances were downgraded in both RI cases. Although highly affected by the properties of the seismic excitation, the prototypes with C2 which were more stiff than C1 oscillated with higher frequencies (Figure 8(b)) and thus developed larger accelerations. This

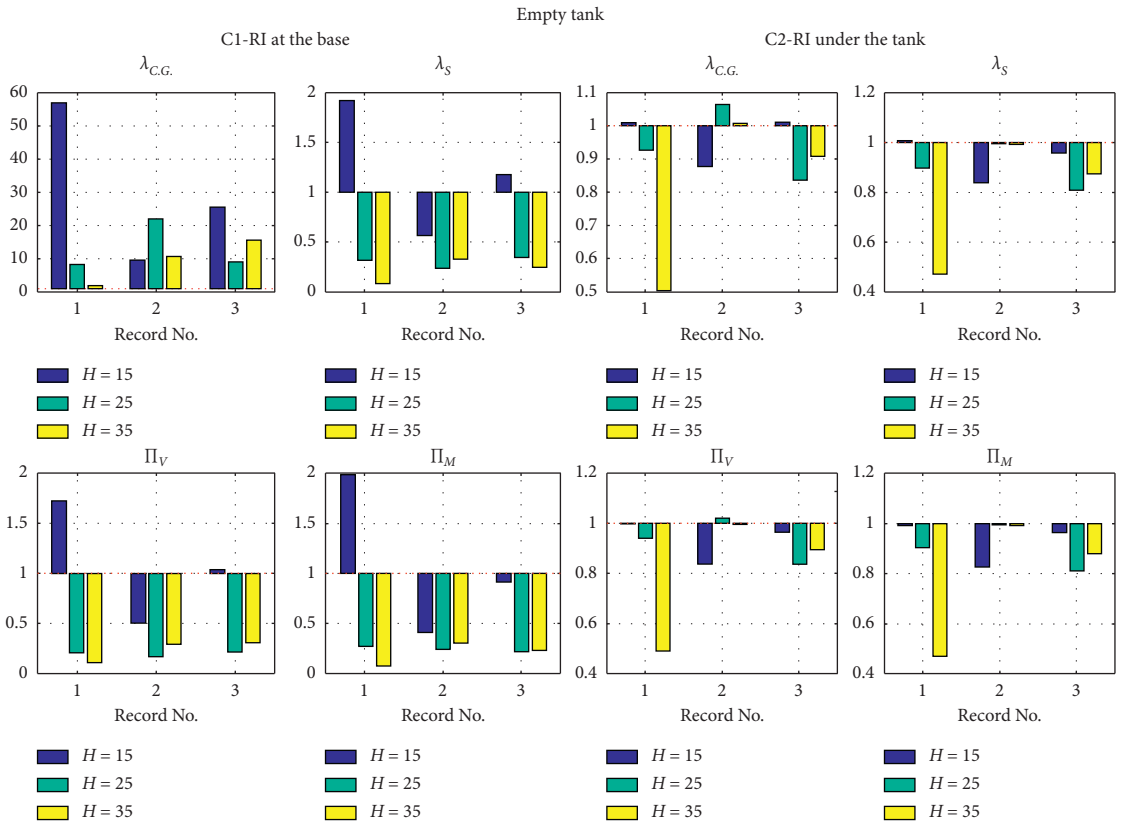

Figure 21: Performance of the prototype structures with "empty tank" and various "shaft heights" (15, 25, and 35 (m)).

resulted in larger wave oscillations (equation (29)). However, in the case of prototypes with C1, wave oscillations were mainly caused by larger rocking responses, rather than amplified accelerations. This phenomenon was also observed in similar rocking structures [10].

(2) "Structural" performances which were described by the shaft response followed the similar pattern of the C.G. displacements. Under the action of the considered ensemble of the seismic motion, the structural performance of C2 prototypes showed almost no advantage over the fixed-base structures ($0.8 < \lambda_S < 1.1$). Similarly, short C1 prototypes (C1-15) experienced such strong impacts and high-frequency oscillations that the displacements became larger than those of the corresponding fixed-base structure ($\lambda_S \approx 1.8$). However, the structural performance of the mid-rise and tall C1 prototypes (C1-25 and C1-35) were upgraded to at least 50%, i.e., decreasing the deformation demands of the shaft to half of the corresponding fixed-base structure ($\lambda_S \leq 0.5$). Thus, the best structural performances were expected from slender prototypes equipped with C1.

(3) As shown in the bottom row of Figures 19–22, the "force" performances followed the similar patterns of the C.G. and shaft displacements. Thus, the force performance ratios were almost equal to those of the structural performances.

7.2. The Effect of Seismic Base Excitations. The effect of earthquake records on the performance of prototype structures was implicitly discussed in previous section. It was shown that the records with predominant ranges of frequencies (or periods) close to the components of the liquid-tank system or the shaft imposed higher demands on these components.

(1) As shown in Figure 17, record no. 2 had higher spectral power around the frequency of the convective component. Thus, it developed larger accelerations and convective responses for stiff prototypes. However, for flexible prototypes, such as those with C1, large convective responses were also developed under the action of record no. 3. This record pair covered a wider range of frequencies and also a stronger vertical component (higher VCS). Thus, it produced larger rocking responses. Same patterns were also observed for C.G. displacements and performances. It was concluded that the operational performances could be more downgraded under the action of the records with wider ranges of dominant frequencies.

(2) The structural performances of the mid-rise and tall C1 prototypes (C1-25 and C1-35), with the highest upgrade ratios, were not affected by the properties of the seismic records. However, the performances of other prototypes were affected by the records predominant ranges of frequencies. For instance, the response of the short C1 prototypes (C1-15) was more affected by record no. 1.

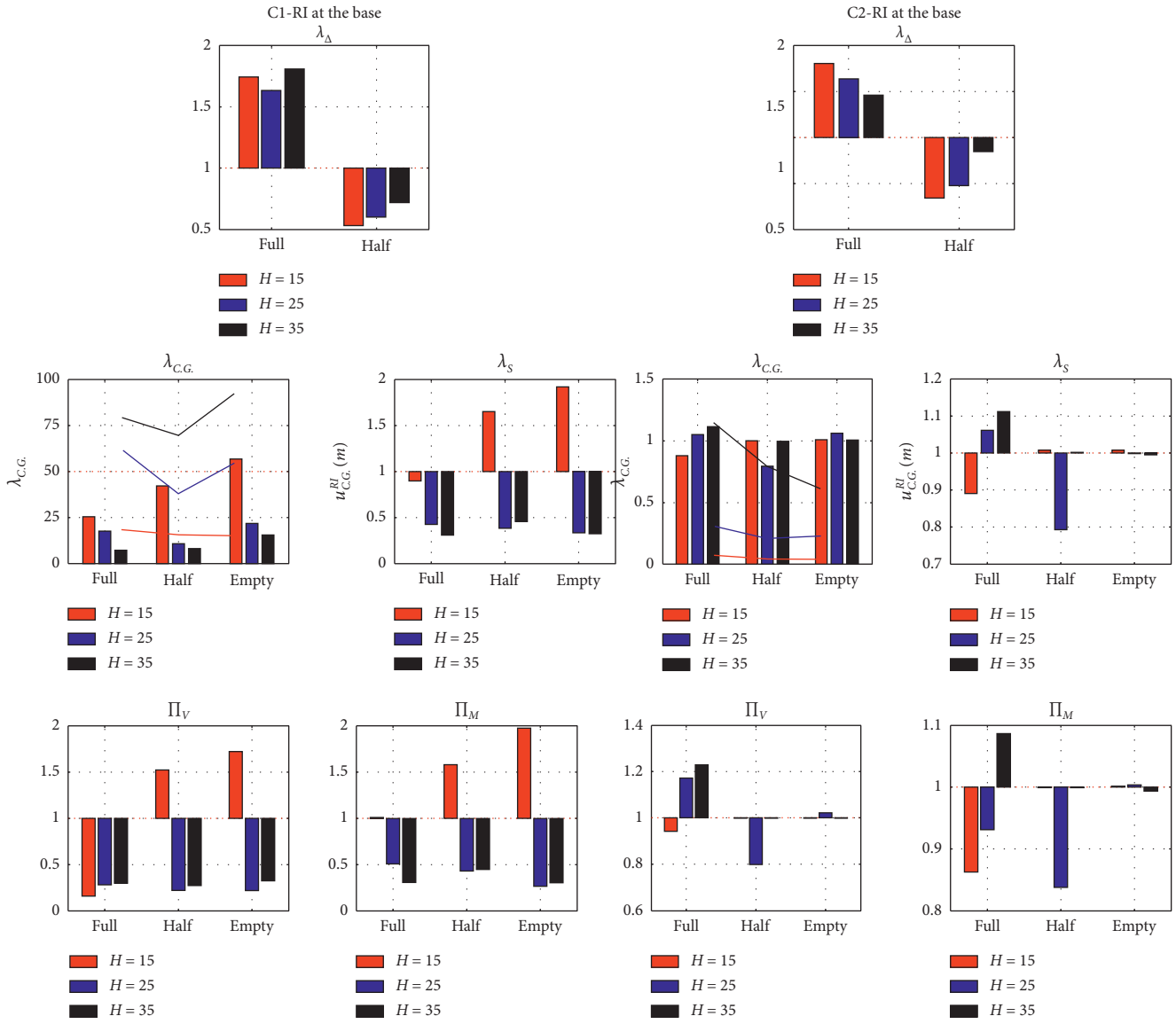

Figure 22: Maximum performance parameters of the prototypes with various "tank filling levels" (full, half, and empty) and "shaft heights" (15, 25, and 35 (m)).

(3) As shown in the bottom row of Figures 19–21, the "force" performances followed the similar patterns of the structural performances and C.G. displacements.

7.3. The Effect of Shaft Heights

(1) As shown in Figures 19–22, various shaft heights had almost no effect on the operational performances. However, the short prototypes with C1 experienced larger C.G. displacements than the corresponding fixed-base structures. This, as described before, was a result of high-frequency oscillations and stronger impacts which is experienced by stiff rocking structures.

(2) The shaft height had almost no effect on the operational performances of the C2 prototypes. However, as discussed before, due to higher stiffness, short C1 prototypes (C1-15) underwent larger shaft displacements than the mid-rise or tall prototypes. The latter demonstrated almost similar performances.

(3) As shown in the bottom row of Figures 19–22, the "force" performances followed the similar patterns of the structural performances and C.G. displacements.

7.4. The Effect of Tank Filling Levels

(1) Various tank fillings levels, as shown in Figure 22, had almost no effect on the operational performances of full tanks. Nevertheless, the prototypes with half tanks experienced lower wave oscillations than those of the corresponding fixed-base structures ($\lambda_\Delta < 1.0$). However, the freeboard allowances must be evaluated based on the results of the full-tank prototypes, which are 1.5–2 times of the required freeboard of the fixed-

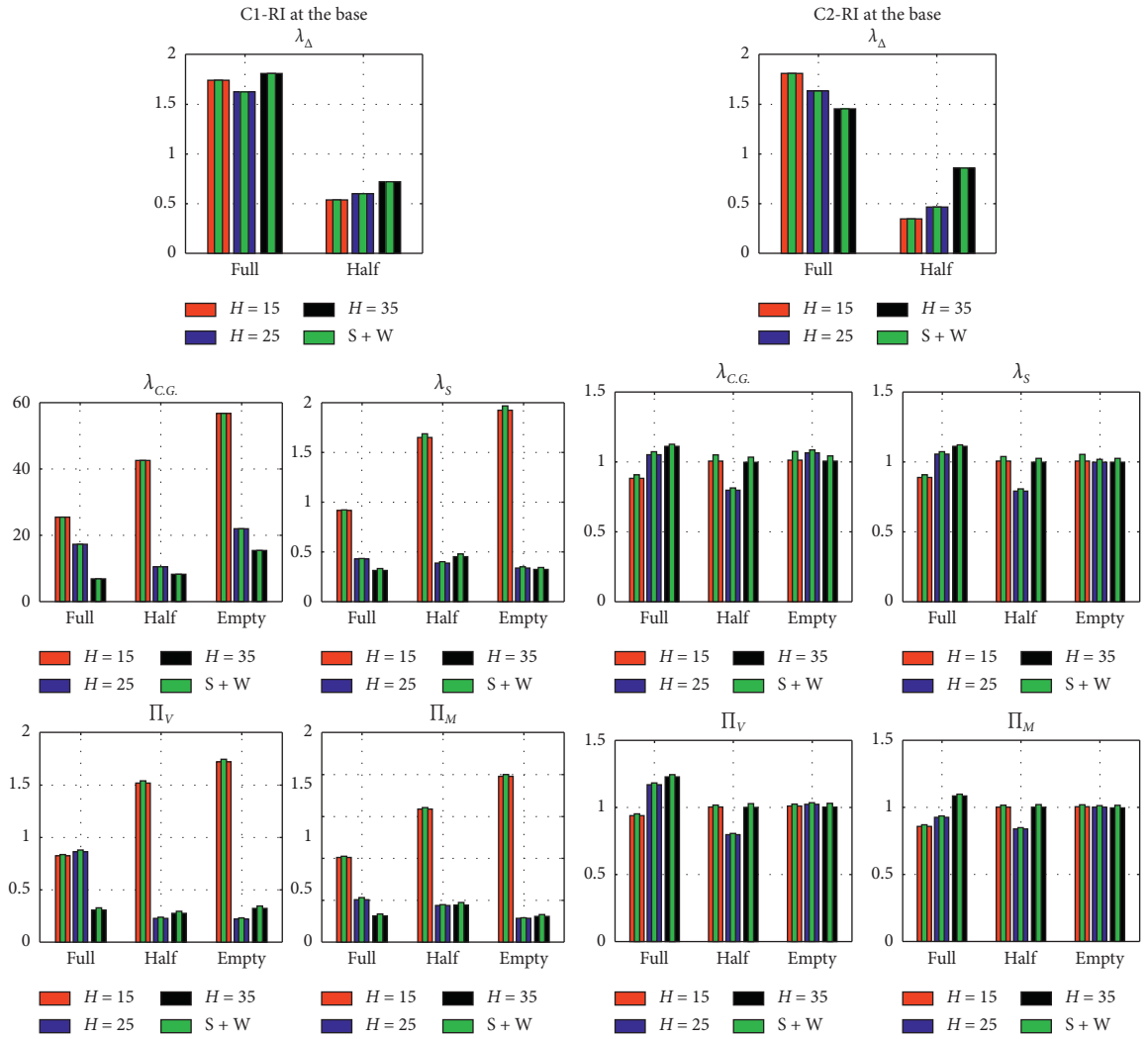

Figure 23: Maximum performance parameters of the prototypes under various lateral load combinations (green bars: seismic + wind).

base structures. It is noteworthy that, as shown in Figure 22 (middle), the full and empty tanks developed almost similar C.G. displacements. Thus, unlike the fixed-base structures, the empty structures should also be considered as a critical design case.

(2) Similarly, various tank fillings had almost no effect on the structural performances of C1 prototypes. However, half and empty short structures (C1-15) experienced larger shaft displacements. The C2 prototypes with half and empty tanks were also not affected by RI.

7.5. The Effect of Combined Seismic and Wind Hazards. The concurrent effect of seismic and wind hazards on the maximum responses of the prototypes is summarized in Figure 23. Moreover, Figure 24 shows the maximum difference ratios of various parameters which were produced under combined loadings. Since the wind loading, as described in Section 6.2, was assumed to act statically, no changes were applied to dynamic responses of system, such as the acceleration. Only the static deformation and displacement of the tank and shaft were superposed with the responses of the seismic loading. Moreover, due to higher stiffness of the tank structure in comparison to the supporting shaft, the tank deformations under wind were also smaller than those of the shaft.

(1) Accordingly, the convective responses and maximum wave oscillations under concurrent seismic and wind loadings ($S + W$) were not modified in comparison to the seismic-only responses. As shown in Figure 24, the maximum ratio of the convective responses was less than 1%, which was produced due to the increased rotation of the liquid-tank system under wind loading.

Similar pattern was observed for the C.G. displacements of the prototypes with C1. Since the tank in C1 is constrained to the shaft, wind loading did not increase C.G. displacement any more. However, considering that the tank is free to rotate in C2, larger rotations than those of the C1 were observed. Thus, the C.G. displacements of C2 prototypes were increased up to 7% under combined loadings.

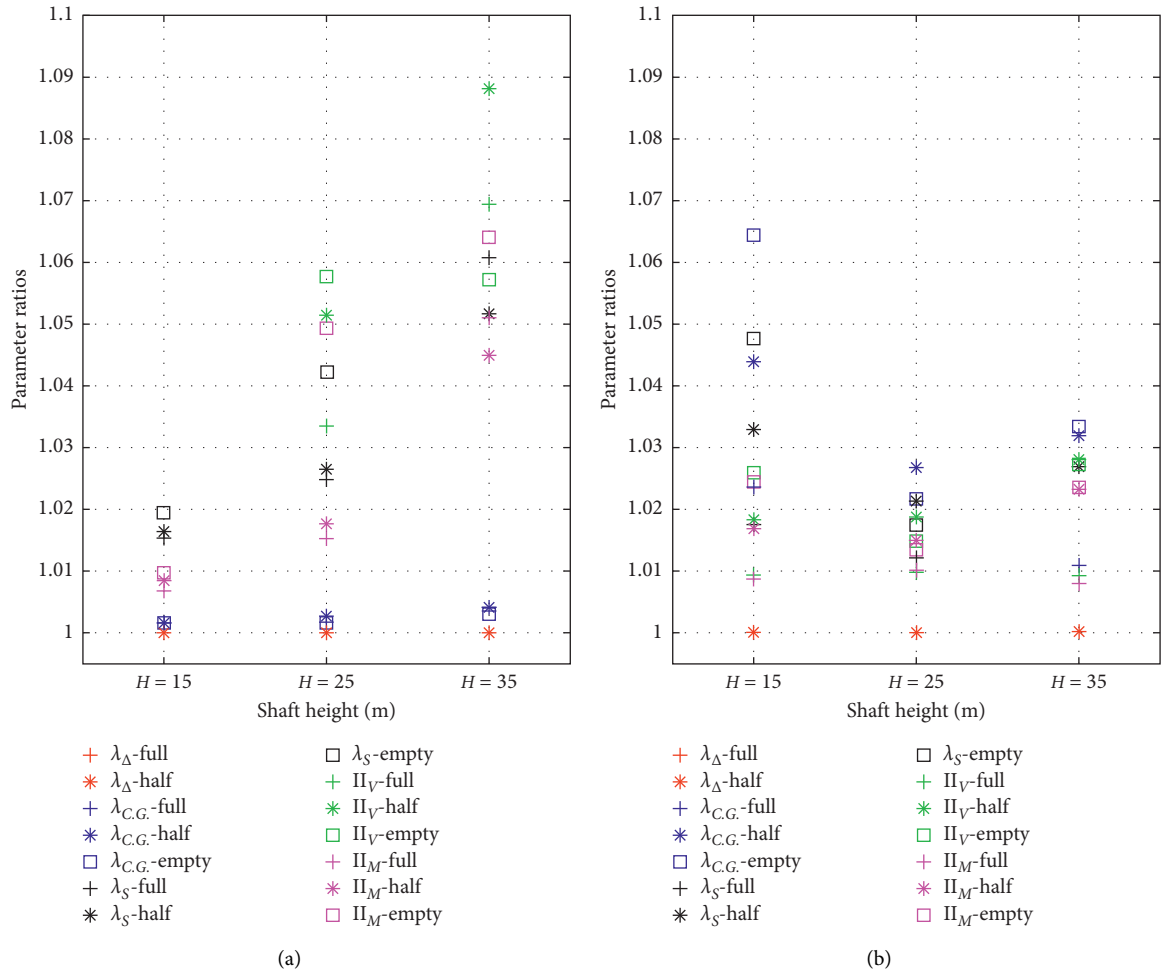

Figure 24: Maximum ratios of various response parameters under the assumed lateral load combinations (seismic + wind/seismic). (a) C1 RI at the base. (b) C2 RI under the tank.

(2) Following a similar pattern, the shaft displacements and structural performance of the C1 prototypes were increased up to 7% under combined loadings. This ratio was about 5% for C2 prototypes.

(3) Considering that the main part of the wind load is acting on the shaft, force performances of C2 prototypes were modified less than 3% under combined loadings. However, for tall structures with C1, the base shear ratio was about 10%, the largest ratio under combined loadings.

8. Conclusions

This paper addressed response mitigation of elevated liquid storage tanks equipped with RI using a developed analytical model. Two different positions of isolation were assumed. The study was carried out for a study group geometrically similar to a real structure, but with various shaft heights, tank materials, and filling levels. Additionally, considering that the system with RI may also be vulnerable to other lateral loadings, the combined effects of seismic and wind loads were also studied in this paper. An unprecedented interacting effect of the convective component and rocking motion was noted for this system which also provided an additional source of energy dissipation. Unlike the other components, frequency decrease was observed for the convective component. This showed that the convective component plays a critical role in seismic analysis of these structures. The effect of RI was then studied on the acceleration response of the system, directly affecting the hydrodynamic pressure, base shear, and base moment demands. Parametric studies showed that the first case of RI (C1) decreases the acceleration demands of slender structures, while C2 had almost no effect on the response. As a result, one could obtain more economic designs for the shaft and foundation of the slender system with C1. Moreover, various shaft heights and tank filling levels had almost no effect on the operational and structural performances. Finally, while the combined seismic and wind hazards had almost no effect on the operational performances, the force performances of the C1 prototypes were increased up to 10%.

It was also shown that earthquake records with strong vertical components aggravate performance of the structures with C1. Additionally, the performance of various components is more intensified by the records with wider ranges of

predominant frequencies. Nevertheless, probabilistic analyses with a higher number of seismic excitations might be needed for a better understanding of the effect of various properties of the earthquake excitations. Finally, some of the short prototypes with half or empty tanks and C1 isolation case undergo such large rocking responses that application of additional restoring systems, such as vertical restrainers, might become a necessity. However, this is the goal of future studies.

Data Availability

The data used to support the findings of this study including the MATLAB script developed for the dynamic analysis are available from the corresponding author upon request.

Conflicts of Interest

The authors declare that there are no conflicts of interest regarding the publication of this paper.

References

[1] Canterbury Earthquakes Royal Commission, "Low-damage building technologies," vol. 3, Canterbury Earthquakes Royal Commission, Christchurch, New Zealand, 2012, Final report.

[2] G. W. Housner, "The behavior of inverted pendulum structures during earthquakes," *Bulletin of the Seismological Society of America*, vol. 53, no. 2, pp. 403–417, 1963.

[3] N. Makris, "A half-century of rocking isolation," *Earthquakes and Structures*, vol. 7, no. 6, pp. 1187–1221, 2014.

[4] A. K. Chopra and S. C. S. Yim, "Simplified earthquake analysis of structures with foundation uplift," *Journal of Structural Engineering*, vol. 111, no. 4, pp. 906–930, 1985.

[5] Q. T. M. Ma, *The Mechanics of Rocking Structures Subjected to Ground Motion*, Ph.D. Dissertation, Department of Civil and Environmental Engineering, University of Auckland, Auckland, New Zealand, 2010.

[6] M. F. Vassiliou and N. Makris, "Analysis of the rocking response of rigid blocks standing free on a seismically isolated base," *Earthquake Engineering & Structural Dynamics*, vol. 41, no. 2, pp. 177–196, 2012.

[7] L. Collini, R. Garziera, K. Riabova, M. Munitsyna, and A. Tasora, "Oscillations control of rocking-block-type buildings by the addition of a tuned pendulum," *Shock and Vibration*, vol. 2016, Article ID 8570538, 11 pages, 2016.

[8] J. A. Bachmann, M. Strand, M. F. Vassiliou, M. Broccardo, and B. Stojadinović, "Is rocking motion predictable?" *Earthquake Engineering & Structural Dynamics*, vol. 47, no. 2, pp. 535–552, 2018.

[9] S. Acikgoz and M. J. DeJong, "The interaction of elasticity and rocking in flexible structures allowed to uplift," *Earthquake Engineering and Structural Dynamics*, vol. 41, no. 15, pp. 2177–2194, 2012.

[10] M. F. Vassiliou, R. Truniger, and B. Stojadinović, "An analytical model of a deformable cantilever structure rocking on a rigid surface: development and verification," *Earthquake Engineering & Structural Dynamics*, vol. 44, no. 15, pp. 2775–2794, 2015.

[11] A. Agalianos, A. Psychari, M. F. Vassiliou, B. Stojadinovic, and I. Anastasopoulos, "Comparative assessment of two rocking isolation techniques for a motorway overpass bridge," *Frontiers in Built Environment*, vol. 3, p. 47, 2017.

[12] R. Truniger, M. F. Vassiliou, and B. Stojadinović, "An analytical model of a deformable cantilever structure rocking on a rigid surface: experimental validation," *Earthquake Engineering & Structural Dynamics*, vol. 44, no. 15, pp. 2795–2815, 2015.

[13] S. Acikgoz, Q. Ma, A. Palermo, and M. J. DeJong, "Experimental identification of the dynamic characteristics of a flexible rocking structure," *Journal of Earthquake Engineering*, vol. 20, no. 8, pp. 1199–1221, 2016.

[14] P. D. Spanos, P. C. Roussis, and N. P. A. Politis, "Dynamic analysis of stacked rigid blocks," *Soil Dynamics and Earthquake Engineering*, vol. 21, no. 7, pp. 559–578, 2001.

[15] V. Drosos and I. Anastasopoulos, "Shaking table testing of multidrum columns and portals," *Earthquake Engineering & Structural Dynamics*, vol. 43, no. 11, pp. 1703–1723, 2014.

[16] J. A. Bachmann, M. F. Vassiliou, and B. Stojadinović, "Dynamics of rocking podium structures," *Earthquake Engineering & Structural Dynamics*, vol. 46, no. 14, pp. 2499–2517, 2017.

[17] G. Simoneschi, A. M. de Leo, and A. Di Egidio, "Effectiveness of oscillating mass damper system in the protection of rigid blocks under impulsive excitation," *Engineering Structures*, vol. 137, pp. 285–295, 2017.

[18] R. D. Sharpe and R. I. Skinner, "The seismic design of an industrial chimney with rocking base," *Bulletin of the New Zealand National Society for Earthquake Engineering*, vol. 16, no. 2, pp. 98–106, 1983.

[19] J. L. Beck and R. I. Skinner, "The seismic response of a reinforced concrete bridge pier designed to step," *Earthquake Engineering & Structural Dynamics*, vol. 2, no. 4, pp. 343–358, 1973.

[20] A. Di Egidio, D. Zulli, and A. Contento, "Comparison between the seismic response of 2D and 3D models of rigid blocks," *Earthquake Engineering and Engineering Vibration*, vol. 13, no. 1, pp. 151–162, 2014.

[21] M. A. Haroun and H. M. Ellaithy, "Model for flexible tanks undergoing rocking," *Journal of Engineering Mechanics*, vol. 111, no. 2, pp. 143–157, 1985.

[22] A. S. Veletsos and Y. Tang, "Rocking response of liquid storage tanks," *Journal of Engineering Mechanics*, vol. 113, no. 11, pp. 1774–1792, 1987.

[23] T. Taniguchi, "Rocking behavior of unanchored flat-bottom cylindrical shell tanks under action of horizontal base excitation," *Engineering Structures*, vol. 26, no. 4, pp. 415–426, 2004.

[24] M. N. Ahari, S. Eshghi, and M. G. Ashtiany, "The tapered beam model for bottom plate uplift analysis of unanchored cylindrical steel storage tanks," *Engineering Structures*, vol. 31, no. 3, pp. 623–632, 2009.

[25] A. Zingoni, "Liquid-containment shells of revolution: a review of recent studies on strength, stability and dynamics," *Thin-Walled Structures*, vol. 87, pp. 102–114, 2015.

[26] M. K. Shrimali and R. S. Jangid, "Earthquake response of isolated elevated liquid storage steel tanks," *Journal of Constructional Steel Research*, vol. 59, no. 10, pp. 1267–1288, 2003.

[27] M. R. Shekari, N. Khaji, and M. T. Ahmadi, "A coupled BE-FE study for evaluation of seismically isolated cylindrical liquid storage tanks considering fluid-structure interaction," *Journal of Fluids and Structures*, vol. 25, no. 3, pp. 567–585, 2009.

[28] M. Moslemi and M. R. Kianoush, "Application of seismic isolation technique to partially filled conical elevated tanks," *Engineering Structures*, vol. 127, pp. 663–675, 2016.

[29] A. Maleki and M. Ziyaeifar, "Sloshing damping in cylindrical liquid storage tanks with baffles," *Journal of Sound and Vibration*, vol. 311, no. 1-2, pp. 372–385, 2008.

[30] H. N. Phan, F. Paolacci, and S. Alessandri, "Fragility analysis methods for steel storage tanks in seismic prone areas," in *Proceedings of the ASME 2016 Pressure Vessels and Piping Conference*, Article ID V008T08A023, American Society of Mechanical Engineers (ASME), Vancouver, Canada, July, 2016.

[31] M. F Vassiliou, K. R. Mackie, and B. Stojadinović, "A finite element model for seismic response analysis of deformable rocking frames," *Earthquake Engineering & Structural Dynamics*, vol. 46, no. 3, pp. 447–466, 2017.

[32] S. Diamantopoulos and M. Fragiadakis, "Seismic response assessment of rocking systems using single degree-of-freedom oscillators," *Earthquake Engineering & Structural Dynamics*, vol. 48, no. 7, pp. 689–708, 2019.

[33] H. Alemzadeh and H. Shakib, "Numerical study on the response of steel ground tanks with free rocking motion under horizontal earthquake excitation," *Journal of Structure and Steel*, vol. 1395, no. 20, pp. 71–79, 2017.

[34] M. W. Hur and T. W. Park, "Performance evaluation of seismic isolation system by installation location in lighthouse structures," *Shock and Vibration*, vol. 2018, Article ID 5751623, 13 pages, 2018.

[35] G. W. Housner, "The dynamic behavior of water tanks," *Bulletin of the Seismological Society of America*, vol. 53, no. 2, pp. 381–387, 1963.

[36] M. A. Haroun, "Vibration studies and tests of liquid storage tanks," *Earthquake Engineering & Structural Dynamics*, vol. 11, no. 2, pp. 179–206, 1983.

[37] ASCE 7, *Minimum Design Loads for Buildings and Other Structures*, vol. 7, American Society of Civil Engineers, Reston, VA, USA, 2016.

[38] R. W. Clough and J. Penzien, *Dynamics of Structures*, Computers and Structures, Inc., Berkeley, CA, USA, 1995.

[39] H. Alemzadeh, *Development of Controlled Rocking and Self-Centering Mechanisms for Improving Seismic Performance of Elevated Water Tanks*, Ph.D. Dissertation, Department of Civil and Environmental Engineering, Tarbiat Modares University, Tehran, Iran, 2019.

[40] J. W. Meek, "Effects of foundation tipping on dynamic response," *Journal of the Structural Division*, vol. 101, no. 7, pp. 1297–1311, 1975.

[41] L. F. Shampine, I. Gladwell, and S. Thompson, *Solving ODEs with Matlab*, Cambridge University Press, New York, NY, USA, 2003.

[42] J. R. Dormand and P. J. Prince, "A family of embedded Runge-Kutta formulae," *Journal of Computational and Applied Mathematics*, vol. 6, no. 1, pp. 19–26, 1980.

[43] A. M. Memari, M. M. Ahmadi, and B. Rezaee, "Behaviour of RC water towers during Manjil-Roudbar earthquake of June 1990," in *Proceedings of the 10th World Conf. on Earthquake Engineering*, Madrid, Spain, July 1992.

[44] ACI 350.3-06, *Seismic design of liquid containing concrete structures and commentary*, American Concrete Institute, Farmington Hills, MI, USA, 2006.

[45] J. B. Mander and C. T. Cheng, *"Seismic Resistance of Bridge Piers Based on Damage Avoidance Design," Technical Report NCEER-97-0014*, Department of Civil, Structural and Environmental Engineering, State University of New York at Buffalo, New York, NY, USA, 1997.

[46] N. H. Hamid and J. B. Mander, "Damage avoidance design for buildings," *KSCE Journal of Civil Engineering*, vol. 18, no. 2, pp. 541–548, 2014.

[47] T. D. Ancheta, R. B. Darragh, J. P. Stewart et al., *Peer NGA-West2 Database*, Pacific Earthquake Engineering Research Center (PEER), University of California, Berkeley, CA, USA, 2013, https://ngawest2.berkeley.edu/.

[48] N. Reggiani Manzo and M. F. Vassiliou, "Displacement-based analysis and design of rocking structures," *Earthquake Engineering & Structural Dynamics*, vol. 48, no. 14, pp. 1613–1629, 2019.

[49] A. G. Davenport, "How can we simplify and generalize wind loads?" *Journal of Wind Engineering and Industrial Aerodynamics*, vol. 54-55, pp. 657–669, 1995.

[50] E. Assareh, M. A. Behrang, M. Ghalambaz, A. R. Noghrehabadi, and A. Ghanbarzadeh, "An analysis of wind speed prediction using artificial neural networks: a case study in Manjil, Iran," *Energy Sources, Part A: Recovery, Utilization, and Environmental Effects*, vol. 34, no. 7, pp. 636–644, 2012.

[51] National Building Regulations, *Part 6 Design Loads for Buildings Part 6-92*, Bureau for compiling and promoting national regulations for buildings, Ministry of Housing and Urbanism, Tehran, Iran, 2013.